UNIVERSITY OF CALIFORNIA

Los Angeles

A Coupled Systems Approach to Solute Transport within a Heterogeneous Vadose Zone-Groundwater Environment

A dissertation submitted in partial satisfaction of the

requirements for the degree Doctor of Philosophy

in Civil Engineering

by

Jason C. Fisher

2005

The dissertation of Jason C. Fisher is approved.

_____
Steven A. Margulis

_____
Lieven Vandenberghe

_____
Thomas C. Harmon

_____
William W-G. Yeh, Committee Chair

University of California, Los Angeles

2005

TABLE OF CONTENTS

LIST OF TABLES

LIST OF FIGURES

NOMENCLATURE

a_L	longitudinal dispersivity (m)
a_M	molecular diffusion coefficient (m^2/d)
a_T	lateral dispersivity (m)
A_{basin}	surface area of the spreading basin (m^2)
A_e	area of triangular elements (m^2)
α	van Genuchten entry pressure (1/m)
B_c	flux boundary (-)
B_d	Dirichlet boundary (-)
B_n	gradient flux boundary (-)
B_v	variable boundary (-)
β	soil specific exponent (-)
c	System 1 time step index (-)
c	cutoff value index (-)
C	material concentration (mg/L)
C_i	prescribed initial concentration condition (mg/L)
C_{in}	effluent concentration (mg/L)
C_v	prescribed concentration of water through the variable boundary (mg/L)
d	System 2 time step index (-)
δ	Kronecker delta tensor (-)
D	dispersion coefficient tensor (m^2/d)
ΔS	change in mass storage for water above the control plane (kg)
Δz	flow path length (m)
e	element index for triangular element mesh (-)
e	element index for prismatic element mesh (-)

E	total number of triangular elements within the control plane (-)
E_1, E_2, E_3, E_4	triangular element identification (-)
E	total number of prismatic elements in System 1 (-)
F	proportion of a given soil type (vol./vol.)
γ	soil specific exponent (-)
h	pressure head (m)
h_d	prescribed pressure head on the Dirichlet boundary (m)
h_i	initial pressure head conditions for the flow equation (m)
h_1, h_2	pressure heads above and below the centroid of the triangular element (m)
$\hat{h}$	average pressure head within an element (m)
i	level of resolution (-)
i	indicator variables (-)
i_{max}	maximum resolution level (-)
j	element index for the current resolution level (-)
j	block mesh node index (-)
k	array of stored element indices for all resolution levels (-)
k	synthetic soil observation index (-)
$\mathbf{K}$	effective hydraulic conductivity tensor (m/d)
K_r	relative hydraulic conductivity (-)
$\mathbf{K_s}$	saturated hydraulic conductivity tensor (m/d)
K_s	saturated hydraulic conductivity (m/d)
m	fluid mass passing through a triangular element during a single time step (kg)
m'	fluid mass passing through a triangular element for a given System 2 time step (kg)
$\tilde{m}'$	constituent mass passing through a triangular element for a given System 2 time step (kg)
m	node index for finite element mesh (-)

m_{low}	lower mass limit in the adaptive time step algorithm (kg)
M	total fluid mass passing through a triangular element over all time (kg)
$\tilde{M}$	cumulative fluid mass passing through the control plane (kg)
M_{hold}	mass placeholder in the adaptive time step algorithm (kg)
M_{low}	lower mass limit in the adaptive spatial mesh algorithm (kg)
M_r	total mass of water infiltrating into System 1 through the spreading basin (kg)
M_{sum}	total fluid mass for a given resolution level (kg)
M_1, M_2, M_3	midpoints of the line segments within a triangle (-)
n	outward unit vector normal to the boundary (-)
N	total number of elements in System 1 (-)
N_1	total number of spatial nodes in System 1 (-)
N_2	total number of spatial nodes in System 2 (-)
N	total number of unique cutoff values (-)
P_1, P_2, P_3	vertices of triangle (-)
P	field site material type proportions (m^3/m^3)
q	fluid flux (m^3/d)
q_c	prescribed flux rate on the flux boundary (m/d)
q_n	prescribed flux rate on the gradient flux boundary (m/d)
q_{max}	maximum infiltration rate (m/day)
θ_e	effective moisture content (m^3/m^3)
θ_r	residual moisture content (m^3/m^3)
θ_s	saturation moisture content (m^3/m^3)
θ_w	moisture content (m^3/m^3)
r	System 2 recharge time step index (-)
R	spatial region of interest (-)
ρ	density of water at 25 ˚C (kg/m^3)

s	material types (-)
t	time (d)
t_1	System 1 time steps (d)
t_2	System 2 time steps (d)
t'_2	System 2 recharge time steps (d)
t_{hold}	time placeholder in the adaptive time step algorithm (d)
tol	maximum percent difference in the adaptive time step algorithm (%)
T_1	total number of time steps in System 1 (-)
T_2	total number of time steps in System 2 (-)
TOL	maximum percent difference in the adaptive spatial mesh algorithm (%)
T_r	total time period of effluent recharge (d)
τ	tortuosity (-)
u	material values associated with the block mesh nodes (-)
$\hat{u}$	material values associated with the synthetic soil observations (-)
$\tilde{u}$	material values at each node in the finite element mesh (-)
v	material type cutoff values (-)
$\mathbf{V}$	Darcy velocity (m/d)
x	distance along the x-axis of a Cartesian coordinate system (m)
y	distance along the y-axis of a Cartesian coordinate system (m)
ψ	capillary pressure head (m)
z	distance along the z-axis of a Cartesian coordinate system (m)
z	potential head (m)
(x, y, z)	spatial coordinate within the domain of the system (m, m, m)
(x_b, y_b, z_b)	spatial coordinate on the boundary (m, m, m)
$\forall$	volume of element (m^3)

ACRONYMS

1D	One-Dimensional
2D	Two-Dimensional
3D	Three-Dimensional
AD	Above Datum
CP	Control Plane
FEMWATER	A Three-Dimensional Finite Element Computer Model for Simulating Density-Dependent Flow and Transport in Variably Saturated Media
RBCA	Recharge Boundary Construction Algorithm
RDRAM	Rambus Dynamic Random Access Memory
REV	Representative Elementary Volume
VS2DT	Variably Saturated 2D Flow and Transport Model

ACKNOWLEDGMENTS

I would like to express my appreciation for the financial support I received for my dissertation work from the American Water Works Association Research Foundation and the Calleguas Municipal Water District (Donald Kendall). In addition, I would like to thank my advisor Thomas Harmon, whose patience and support proved essential to the completion of this dissertation.

VITA

July 12, 1971	Born, Los Angeles, California
1998	B. S., Environmental Resources Engineering Humboldt State University Humboldt, California
2000	M. S., Environmental Systems Humboldt State University
1997-2001	Hydrologic Technician / Computer Programmer USDA Forest Service Pacific Southwest Research Station, RSL Humboldt, California
2001-2002	Teaching Assistant University of California, Los Angeles Department of Civil and Environmental Engineering
2003	M. S., Civil Engineering University of California, Los Angeles
2002-2004	Graduate Research Assistant University of California, Los Angeles Department of Civil and Environmental Engineering
2004-2005	Research Assistant University of California, Merced School of Engineering Merced, California

PUBLICATIONS AND PRESENTATIONS

Fisher, Jason C. 2000. Simulation of Partially Saturated - Saturated Flow in the Caspar Creek E-Road Groundwater System. Arcata, CA, Humboldt State University, 107 p. M. S. thesis.

American Geophysical Union (AGU) Chapman Conference on State-of-the-Art in Hillslope Hydrology, Sunriver, Oregon, October 8th - 12th 2001. Poster presentation of M.S. thesis research.

American Water Resources Association (AWRA) Annual Water Resources Conference, San Diego, California, November 8th 2003. Presentation on the Modeling of Conjunctive Use Systems Impacted by Natural Sources of Groundwater Contamination.

AGU Fall Meeting, San Francisco, California, December 15th 2004. Poster presentation of Ph.D. dissertation research.

ABSTRACT OF THE DISSERTATION

A Coupled Systems Approach to Solute Transport within a Heterogeneous Vadose Zone-Groundwater Environment

by

Jason C. Fisher

Doctor of Philosophy in Civil Engineering

University of California, Los Angeles, 2005

Professor William W-G Yeh, Chair

A coupled systems approach is presented for the simulation of fluid flow and solute transport within a heterogeneous vadose zone-groundwater environment. Separate model domains were developed for the vadose and saturated zones. The numerical model used is FEMWATER, a three-dimensional (3D) finite element model for simulating flow and transport in variably saturated media. A control plane (CP), normal to the mean flow direction, couples the two systems. The fluid flux and solute

mass passing through the CP during a vadose zone simulation is used to construct the recharge boundary condition in the saturated system. Coupling the two systems allows for the accurate representation of flow and transport within the vadose zone while maintaining the ability to simulate regional plume migration in the saturated zone. The coupling approach is referred to as the Recharge Boundary Construction Algorithm (RBCA). The RBCA adaptively reconciles both the spatial and temporal discretization differences between the vadose zone and saturated zone models.

The accuracy of the RBCA is determined by a set of user-defined parameters controlling the algorithm's adaptive spatial mesh and adaptive temporal time step routines. The routines are designed to capture the greatest resolution of spatial and temporal changes in fluid flux across the CP during a vadose zone simulation. A sensitivity analysis performed on the control parameters for the construction of the recharge boundary shows the maximum percent difference in total mass passing through the CP during a vadose zone simulation as having the greatest effect on the boundary's level of resolution. Numerical simulations are made investigating the impact of effluent recharge at the ground surface on the solute temporal (breakthrough) behavior and spatial distribution in the two systems.

The usefulness of the RBCA method is in its ability to accurately describe the groundwater fluxes across the vadose zone – saturated zone interface (a.k.a. the recharge boundary condition). The method is most applicable for modeling the transport of contaminants from sources originating at the ground surface or within the vadose zone, where the potential for aquifer contamination exists. Specific systems that

could benefit from the decoupled systems approach include those associated with artificial recharge, aquifer storage and recovery, and disposal of wastes by land or pond application.

1 INTRODUCTION

Traditionally, water resources engineers have focused their efforts on simulating groundwater flow and transport within the saturated zone with little attention given to flow processes within the overlying vadose zone. Avoiding of the vadose zone has often required the use of simplifying assumptions to account for the model's inability to simulate contaminant sources located at the ground surface. For example, ground surface contaminant sources are commonly represented using point sources within the saturated zone. While this technique reduces the complexity of the model, it does, however, require estimations of location, recharge rate and solute concentration of the point sources. Furthermore, any information pertaining to the true ground surface contaminant source (e.g. solute concentrations, infiltration rates, land application area) is not directly admissible within the model. The translation of ground surface observations to point source conditions is susceptible to misinterpretation due to the complexities of flow and transport within the vadose zone.

To illustrate the issues surrounding vadose zone-groundwater modeling a hypothetical system (Figure 1.1) is introduced describing effluent land surface application. Effluent is placed within a spreading basin where pressure head differences cause the contaminated water to infiltrate into the subsurface. The wetting front progresses downward through the vadose zone toward the water table and enters the underlying unconfined aquifer. Within the aquifer the effluent forms a contaminant plume where the plume's shape and migration path are controlled by the aquifers flow regime. The driving forces behind the flow regime are base flow and groundwater

mounding beneath the spreading basin. To simulate the movement of effluent through the vadose zone-groundwater environment requires a conceptual model that incorporates infiltration, percolation, mounding and plume migration. The difficulties associated with modeling percolation and plume migration are addressed within this dissertation along with a methodology for overcoming those challenges.

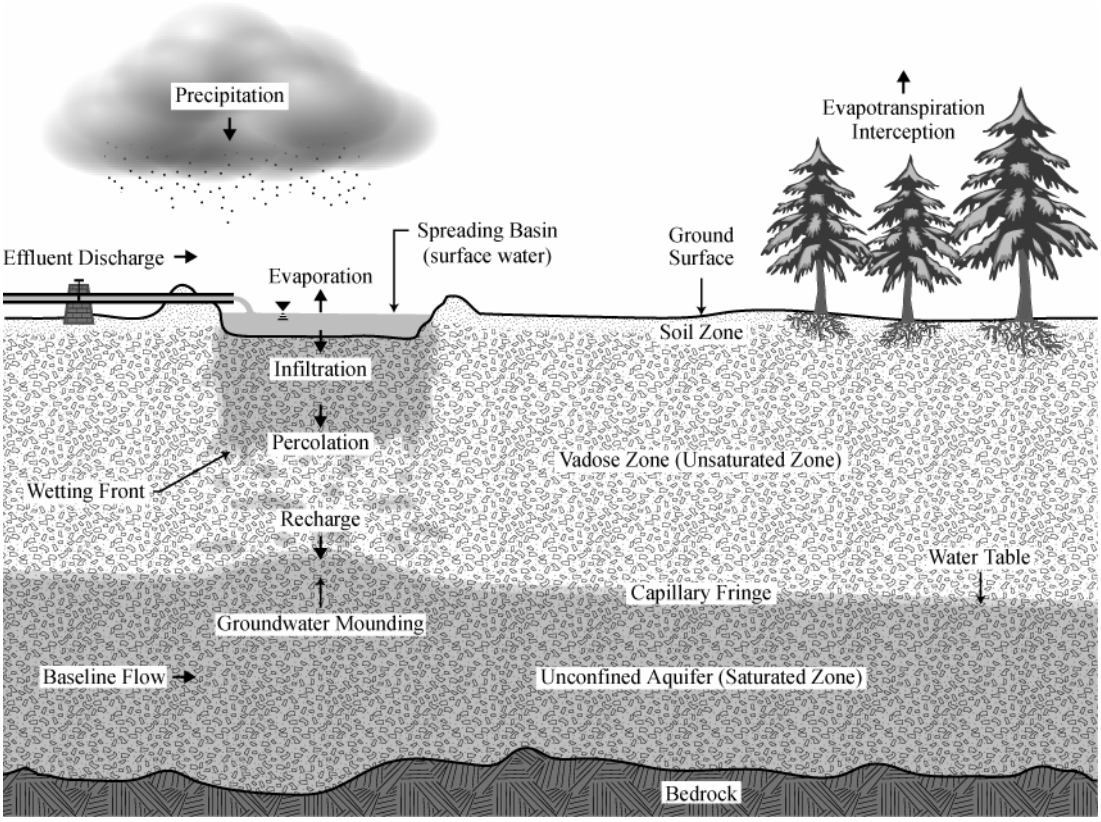

Figure 1.1: Conceptual illustration of effluent infiltration and recharge within a groundwater system.

The computational requirements for modeling flow and transport under partially saturated conditions are much greater than those required for saturated conditions. The higher computational requirements are attributed to the nonlinear governing equations that characterize partially saturated behavior. To accommodate the nonlinearities, thus

facilitating non-convergence during the iterative solution process, an increase in the resolution of the models spatial and temporal discretization must be made. The increase in resolution, however, has the undesirable effect of increasing the computational time required for a simulation. The added computational time all but eliminates the possibility for modeling both percolation and plume migration within a single numerical simulation. An examination of the computational costs associated with a single system approach reveals the method's shortcomings.

At every time step within a numerical model, flow and transport equations must be solved for every node within the models finite element mesh. These repetitive solutions constitute the dominant computational cost associated with any numerical model. Use of a single numerical model to simulate flow and transport within the unsaturated-saturated system requires two distinct nodal resolutions within the finite element mesh. Partially saturated flow within the vadose zone necessitates a much higher nodal density than saturated flow within the unconfined aquifer. Furthermore, the spatial domain required to capture the flow dynamics of percolation beneath the spreading basin is much smaller than the spatial requirements for plume migration. For example, percolation through the vadose zone is typically modeled on the scale of meters whereas plume migration through the unconfined aquifer is frequently modeled on scales of 10s of meters to even kilometers (for regional domains).

Combining the two spatial domains within a single finite element mesh is far from impossible with the use of a sophisticated mesh generation algorithm. However, the real challenge is the use of a single temporal discretization for modeling both percolation and

plume migration. Similar to the constraints on spatial discretization, a small time step is required for modeling partially saturated flow through the vadose zone. Effluent infiltration is typically periodic in nature with cycles occurring a few days out of the month or a few months out of the year. In the single system approach the computational cost incurred by a finer time step resolution is deemed acceptable during periods of recharge when effluent passes through the vadose zone, redistributes, and enters into the underlying aquifer. Under this scenario, the finer temporal discretization permits the simulation of percolation through the vadose zone as well as enabling an accurate representation of the effluent as it enters into the unconfined aquifer.

It is during periods of inactivity for percolation or plume migration that the costs in computational time become unacceptable. For example, during the initial cycle of effluent infiltration, when the wetting front moves downward towards the water table, the nodes within the unconfined aquifer have little influence over the movement of effluent within the vadose zone. Furthermore, the smaller time steps required for modeling partially saturated flow within the vadose zone must also be applied to the superfluous nodes within the unconfined aquifer. When flow within the vadose zone has all but ceased and the movement of effluent is completely contained within the unconfined aquifer, the nodes within the vadose zone no longer contribute to the movement of effluent. The saturated conditions within the unconfined aquifer allow for a much larger time step, however, the governing equations for flow and transport must still be solved at every node within the system. During this time the nodes within the vadose zone can only be viewed as a computational burden to the simulation.

The traditional method (Hantush, 1967) for addressing the complexities of unsaturated-saturated modeling is to neglect the flow within the vadose zone, thus eliminating flow and transport through the partially saturated media. Neglecting vadose zone flow requires a change in location for the effluent source. The effluent no longer enters the system through the spreading basin but is rather injected into the unconfined aquifer at nodal point(s) within the water table. The movement of effluent is then contained within the saturated media of the unconfined aquifer. The obvious advantage to this approach is the coarse spatial and temporal discretizations afforded by the saturated conditions. Disadvantages to the approach are the inherent inaccuracies introduced to the model when neglecting infiltration and percolation processes.

The objective of this dissertation is to present a method for circumventing the challenges associated with a single system approach while avoiding the oversimplifying assumptions that could potentially compromise the accuracy of the model. The working hypothesis behind the method is that an accurate and computationally efficient flow and transport simulation can be achieved by decoupling the unsaturated-saturated system into two separate numerical models. The first model simulates percolation within the vadose zone while the second model simulates plume migration within the unconfined aquifer. Decoupling the system necessitates the construction of a recharge boundary condition for the unconfined aquifer based on the output of a vadose zone simulation. The details of the method are presented within the body of this dissertation. In Chapter 2 a summary is made of literature pertaining to unsaturated-saturated modeling. Chapter 3 addresses the formulation and development of the numerical models. In Chapter 4 the Recharge

Boundary Construction Algorithm (RBCA) is developed. Finally, the results and conclusions are presented in Chapters 5 and 6, respectively.

2 LITERATURE REVIEW

The effect's of natural or artificial recharge on groundwater systems has been studied extensively over the past half century. Research has primarily focused on the development and implementation of predictive models to describe the movement of groundwater subject to recharge. Early research focused on analytical solutions based on idealized aquifer systems. In later research, stochastic and numerical methods were implemented to allow for greater complexity in groundwater systems with input variables that varied in space and time (e.g. transient recharge).

Analytical solutions describing the variation of the water table within an infinite aquifer in response to recharge from rectangular and circular basins were obtained by Hantush (1967). Hantush's solutions are based on Dupuit assumptions and neglect the effects of the unsaturated zone. Numerical and algebraic approximations of Hantush's mound function are given by Marino (1975), and Swamee and Ojha (1997), respectively. Rao and Sarma (1983) obtained a solution for the prediction of water table fluctuations within a finite aquifer subject to constant recharge from a finite rectangular basin and a strip basin of infinite length. Latinopoulos (1986) studied the same problem for rectangular aquifers but subjected to a varying recharge regime. The significant effect of time varying recharge on water table fluctuations was observed by Zomorodi (1991) and Rai and Singh (1995). Serrano (1992) showed that groundwater recharge from the

unsaturated zone generates a variable velocity field that may considerably influence solute transport in the saturated zone.

An approximate 3D analytical model using vertical and radial coordinates was developed by Morel-Seytoux and others (1990) to predict unsaturated aquifer recharge from a circular spreading basin. Zlotnik and Ledder (1992, 1993) demonstrate the use of analytical formulas for unsteady hydraulic head and velocity components in an unconfined aquifer of finite thickness with a circular and rectangular source of recharge. Manglik and Rai (1998, 2000) developed an analytical solution to the linearized Boussinesq equation to predict the variation of the water table in response to time-varying recharge applied through single and multiple rectangular basins. Rai and others (2001) extended the work of Manglik and Rai to incorporate recharge form strip basins for any number of recharge cycles.

Stochastic solutions based on a Lagrangian flux approach were first presented by Rubin and Bellin (1994) for uniformly distributed recharge in a heterogeneous porous media. The purpose of their study was to investigate the effects of groundwater recharge from the unsaturated zone on the statistics of solute velocity in the saturated zone. The use of the Lagrangian flux approach is again seen in the work of Destouni and Graham (1995). They derived an approximate analytic expression for field-scale solute breakthrough in a coupled flow problem utilizing a joint probability density function between the travel times in the two zones. The coupling between the unsaturated and saturated zones is not fully accounted for in that the two flow regimes are solved

separately, and the mean flow in the unsaturated zone is set to be vertical while that in the saturated zone is taken to be horizontal.

Additional stochastic studies include an investigation by Li and Yeh (1998) of the sensitivity, the head variance and the cross-correlation functions of the log hydraulic conductivity and pressure head for transient flow in a saturated-unsaturated system with a vector state-space approach. Sun and Zhang (2000) investigate the effects of a water table boundary on solute spreading in an unsaturated porous medium with unidirectional nonstationary flow field. They found that near the water table the longitudinal displacement covariance decreases. A method of moments approach conducted by Zhang and Lu (2002) show that flow nonstationarity may be caused by nonstationary medium properties, complex flow configurations, or appropriate boundary conditions, such as a water table boundary. Lu and Zhang (2003) then developed a general model to predict the displacement covariance tensor for solute transport in a nonstationary flow field, in which both the mean flow direction and magnitude may vary in space.

A commonly used 2D finite difference model for the prediction of flow and transport in a saturated-unsaturated system subject to recharge is VS2DT (Lappala et al., 1987; and Healy, 1990). Sumner and Bradner (1996) demonstrate that the saturated-unsaturated flow equation (VS2DT) is adequate for describing field-measured groundwater mounding beneath an infiltration basin. McCord and others (1997) implement VS2DT to assess the impacts of geologic heterogeneity on groundwater recharge estimates derived from environmental tracers. They found that recharge inferred using environmental tracer methods is highly spatially variable, tends to

overestimate recharge, and should be considered accurate only to within an order of magnitude, particularly in situations with significant media heterogeneity. Sumner and others (1999) compared methods used to estimate groundwater mounding by comparing an analytical approach (Hantush) with a numerical approach (VS2DT). The error associated with the analytical methods neglect of the unsaturated zone increases as the basin-loading period is shortened, as the depth to the water table increases, with increasing subsurface anisotropy, and with the inclusion of fine-textured strata. Foussereau and others (2001) studied transport of nonreactive solutes through a coupled, 2D randomly heterogeneous unsaturated-saturated zone system with temporally random rainfall using Monte Carlo simulation results with theoretical results of Destouni and Graham (1995). Russo and others (2001) conduct numerical simulations of water flow and transport in a 3D heterogeneous combined vadose zone-groundwater system. Their analysis indicates that the spreading and the breakthrough of the solute pulse are considerably affected by the recharge at the soil surface.

The research presented in this dissertation offers a new approach for modeling flow and transport in a vadose zone-groundwater system. The 3D numerical solution is designed to capture the unique processes of flow and transport in the vadose zone and saturated zone while preserving the mass transfer between the two subregions. Decoupling the two subregions allows for the simulation of regional plume migration based on accurate estimates of recharge. The approach developed here will be useful in studying a host of problems in the fields of environmental engineering, water resources management, and hydrogeologic science. Specific systems that could benefit from the

decoupled systems approach include those associated with artificial recharge, aquifer storage and recovery, and disposal of wastes by land or pond application.

3 MODEL FORMULATION AND DEVELOPMENT

The ability to model any groundwater system is limited by our understanding of the physical hydrologic processes, the ability to describe the hydrogeology within the field site, and the computational power of the day. These limitations, as they apply to an unsaturated-saturated system, were considered throughout the process of model selection. The model decided upon is FEMWATER (Lin et al., 1997), a 3D finite element code for simulating both flow and transport through unsaturated-saturated media. Flow is described with a modified version of the Richards equation (Richards, 1931):

$$\left(\frac{\partial \theta_w}{\partial h}\right)\frac{\partial h}{\partial t} = \nabla \cdot \left[\mathbf{K} \cdot \left(\nabla h + \nabla z\right)\right] \tag{3.1}$$

where θ_w is the moisture content, h is the pressure head; t is time, z is the potential head, and **K** is the effective hydraulic conductivity tensor. The effective hydraulic conductivity is defined as

$$\mathbf{K} = K_r \, \mathbf{K_s} \tag{3.2}$$

where K_r is the relative hydraulic conductivity and $\mathbf{K}_s$ is the saturated hydraulic conductivity tensor. Equation 3.2 rewritten in matrix notation and assuming isotropic conditions is expressed as

$$\begin{bmatrix} K_{xx} & K_{xy} & K_{xz} \\ K_{yx} & K_{yy} & K_{yz} \\ K_{zx} & K_{zy} & K_{zz} \end{bmatrix} = K_r \cdot \begin{bmatrix} K_{s,x} & 0 & 0 \\ 0 & K_{s,y} & 0 \\ 0 & 0 & K_{s,z} \end{bmatrix} = K_r \cdot \begin{bmatrix} K_s & 0 & 0 \\ 0 & K_s & 0 \\ 0 & 0 & K_s \end{bmatrix}. \tag{3.3}$$

The relative hydraulic conductivity and moisture content are described using the Mualem-van Genuchten model (Mualem, 1976; van Genuchten, 1980):

$$K_r = \theta_e^{0.5}\left[1-\left(1-\theta_e^{1/\gamma}\right)^{\gamma}\right]^2 \tag{3.4}$$

where

$$\theta_e = \begin{cases}\left[1+\left(|\alpha h|\right)^{\beta}\right]^{-\gamma} & \text{for } h < 0 \\ 1 & \text{for } h \geq 0\end{cases} \tag{3.5}$$

$$\gamma = 1-\frac{1}{\beta} \tag{3.6}$$

and

$$\theta_w = \theta_r + \theta_e \cdot \left(\theta_s - \theta_r\right). \tag{3.7}$$

Where β and γ are soil-specific exponents, α is a soil-specific coefficient, θ_e is the effective moisture content, θ_r is the residual moisture content, and θ_s is the saturation moisture content. The initial conditions for the flow equation are given as

$$h = h_i\left(x, y, z, t = 0\right) \quad \text{in } R, \tag{3.8}$$

where R is the region of interest and h_i is the prescribed initial pressure head condition. The boundary conditions for the flow equation are given in the following equations:

(a) Dirichlet conditions,

$$h = h_d\left(x_b, y_b, z_b, t\right) \quad \text{on } B_d, \tag{3.9}$$

(b) flux conditions,

$$-\mathbf{n}\cdot\mathbf{K}\cdot\left(\nabla h + \nabla z\right) = q_c\left(x_b, y_b, z_b, t\right) \quad \text{on } B_c, \tag{3.10}$$

(c) gradient flux conditions,

$$-\mathbf{n}\cdot\mathbf{K}\cdot\nabla h = q_n\left(x_b, y_b, z_b, t\right) \quad \text{on } B_n, \tag{3.11}$$

where (x_b, y_b, z_b) is the spatial coordinate on the boundary, **n** is the outward unit vector normal to the boundary, B_d is the Dirichlet boundary, B_c is the flux boundary, B_n is the gradient flux boundary, h_d is the prescribed pressure head on the Dirichlet boundary, q_c is the prescribed flux rate on the flux boundary and q_n is the prescribed flux rate on the gradient flux boundary.

The flow equation is solved using the Galerkin finite element methodology. The Galerkin method is one of the methods of weighted residuals, a technique for obtaining an approximate solution to several classes of differential equations. The method uses an approach that transforms the differential equation into a set of algebraic equations. The solution to the algebraic equations gives information about the solution of the original differential equation.

The governing equation for transport is derived from the continuity of mass and flux laws (Aris, 1962). The major processes are advection and dispersion/diffusion. The transport equation is given as

$$\theta_w \frac{\partial C}{\partial t} + \mathbf{V}\cdot\nabla C - \nabla\cdot\left[\mathbf{D}\cdot\nabla C\right] = \left(\frac{\partial\theta_w}{\partial h}\cdot\left(\frac{\partial h}{\partial t}\right) + \nabla\mathbf{V} - \frac{\partial\theta_w}{\partial t}\right)C \tag{3.12}$$

where C is the material concentration in the aqueous phase, **D** is the dispersion coefficient, and **V** is the Darcy velocity. The Darcy velocity (Darcy, 1856) is calculated as follows

$$\mathbf{V} = -\mathbf{K} \cdot \left(\nabla h + \nabla z \right). \tag{3.13}$$

The dispersion coefficient tensor given in Equation (3.12) is defined as

$$\mathbf{D} = \frac{a_T |\mathbf{V}| \delta}{\theta_w} + \left(\frac{a_L - a_T}{\theta_w} \right) \left(\frac{\mathbf{V}\mathbf{V}}{|\mathbf{V}|} \right) + a_M \tau \delta \tag{3.14}$$

where δ is the Kronecker delta tensor; a_T is the lateral dispersivity; a_L is the longitudinal dispersivity; a_M is the molecular diffusion coefficient and τ is the tortuosity. The initial conditions for the transport equation are given by

$$C = C_i \left(x, y, z, t = 0 \right) \quad \text{in R}, \tag{3.15}$$

where C_i is the prescribed initial concentration values. Transport boundary conditions are given in the following equations:

(a) gradient flux conditions,

$$\mathbf{n} \cdot \left(-\mathbf{D} \cdot \nabla C \right) = q_n \left(x_b, y_b, z_b, t \right) \quad \text{on } B_n \tag{3.16}$$

(b) variable conditions,

$$\begin{aligned} \mathbf{n} \cdot \left(\mathbf{V}C - \mathbf{D} \cdot \nabla C \right) &= \mathbf{n} \cdot \mathbf{V} C_v \left(x_b, y_b, z_b, t \right) \quad \text{if } \mathbf{n} \cdot \mathbf{V} \le 0 \quad \text{on } B_v \\ \mathbf{n} \cdot \left(\mathbf{V}C - \mathbf{D} \cdot \nabla C \right) &= 0 \quad \text{if } \mathbf{n} \cdot \mathbf{V} > 0 \quad \text{on } B_v \end{aligned} \tag{3.17}$$

where B_v is the variable boundary and C_v is the prescribed concentration of the water through the variable boundary.

The transport equation is solved using the hybrid Lagrangian-Eulerian finite element methodology; a technique well suited for advection-dominated simulations. The Lagrangian-Eulerian algorithm divides the solution of the transport problem into two steps. The first step uses particle tracking to solve the advective portion of the transport

equation. The second step uses a Eulerian approach to solve the remaining dispersive portion. The algorithm repeatedly alternates between these two steps to obtain solute concentrations at discrete points and times (Ruan and McLaughlin, 1999).

3.1 Flow and Transport Simulations Overview

The unsaturated-saturated system is decoupled into two separate models (System 1 and System 2). System 1 models flow and transport through the vadose zone while System 2 models plume migration within the unconfined aquifer. The schematics for System 1 and 2 are shown in Figure 3.1. The square prism spatial domain of System 1 has spatial dimensions of 6 m by 6 m by 5 m in the x, y and z coordinate directions, respectively. The upper boundary of System 1 is located at the ground surface (12.5 m AD). The lower boundary of System 1 is located at a depth of 5 m below the ground surface (7.5 m AD). Intersecting the lower half of System 1 is the square prism spatial domain of System 2. The horizontal intersection of the two systems occurs at $2\ m \leq x \leq 8$ m and $2\ m \leq y \leq 8$ m. The dimensions of System 2 are 25 m by 10 m by 10 m in the x, y and z coordinate directions, respectively. The base of System 2 is located at datum and representative of an impermeable bedrock surface.

A System 1 simulation is independent of a System 2 simulation; however, the upper recharge boundary condition of System 2 (10 m AD) is dependent on the results of a System 1 simulation. Construction of the System 2 recharge boundary condition is summarized here with a more detailed explanation given in Chapter 4. A horizontal CP (A-A), normal to the mean flow direction, is established where the System 1 spatial

domain intersects the System 2 upper boundary. The fluid flux and concentration passing through the CP are calculated using the spatial-temporal distributions of pressure heads and concentrations from a System 1 simulation. A translation of fluid flux and concentration from System 1 to System 2 is accomplished by reconciling the differences between the spatial and temporal discretizations for the two systems.

The decoupled systems approach assumes that groundwater flow within System 1 is unaffected by fluctuations in the water table. For example, groundwater mounding is assumed to have negligible effects on the flow rates and spatial distribution of groundwater within System 1. Any pressure head feedback from System 2 to System 1 is alleviated by incorporating into System 2 a thin layer of the vadose zone just above the water table. The vertical thickness of the vadose zone layer ($\approx$ 0.8 m) was determined from preliminary System 2 simulations observing the height of groundwater mounding for a range of potential recharge scenarios. Groundwater flow within System 1 may then be characterized solely as gravity drainage. The lower boundary of System 1 is located well beneath the CP (7.5 m AD) to avoid the boundaries influence over the System 1 pressure head distribution. The sensitivity of the RBCA to changes in the System 1 lower boundary location is explored within Chapter 5.

The complexity of the unsaturated-saturated system is further reduced with the following assumptions: (a) no rainfall during the duration of a simulation, (b) water losses due to evapotranspiration are negligible, (c) no flow within the soil zone, (d) no hysteresis effects, (e) the infiltration rate within the spreading basin is uniform, (f) the compressibility of water and medium are zero, (g) the fluid density and dynamic viscosity

remain constant over space and time, and (h) the effluent solute is modeled as a single non-reactive conservative constituent.

Table 1 summarizes the transport properties for the numerical models. The table gives values for tortuosity, longitudinal dispersivity, lateral dispersivity and molecular diffusion coefficient. Transport values were based on realistic field conditions.

Table 1: Transport properties.

Description	Symbol	Value	Units	Reference
tortuosity	τ	0.7	-	Bear, 1988
longitudinal dispersivity	a_L	0.002	m	Russo et al., 2001
lateral dispersivity	a_T	0.0001	m	Russo et al., 2001
molecular diffusion coefficient	a_M	0.000175[†]	m^2/day	Cussler, 1984

[†] Chloride (Cl^-) ions in water at infinite dilution and 25° C

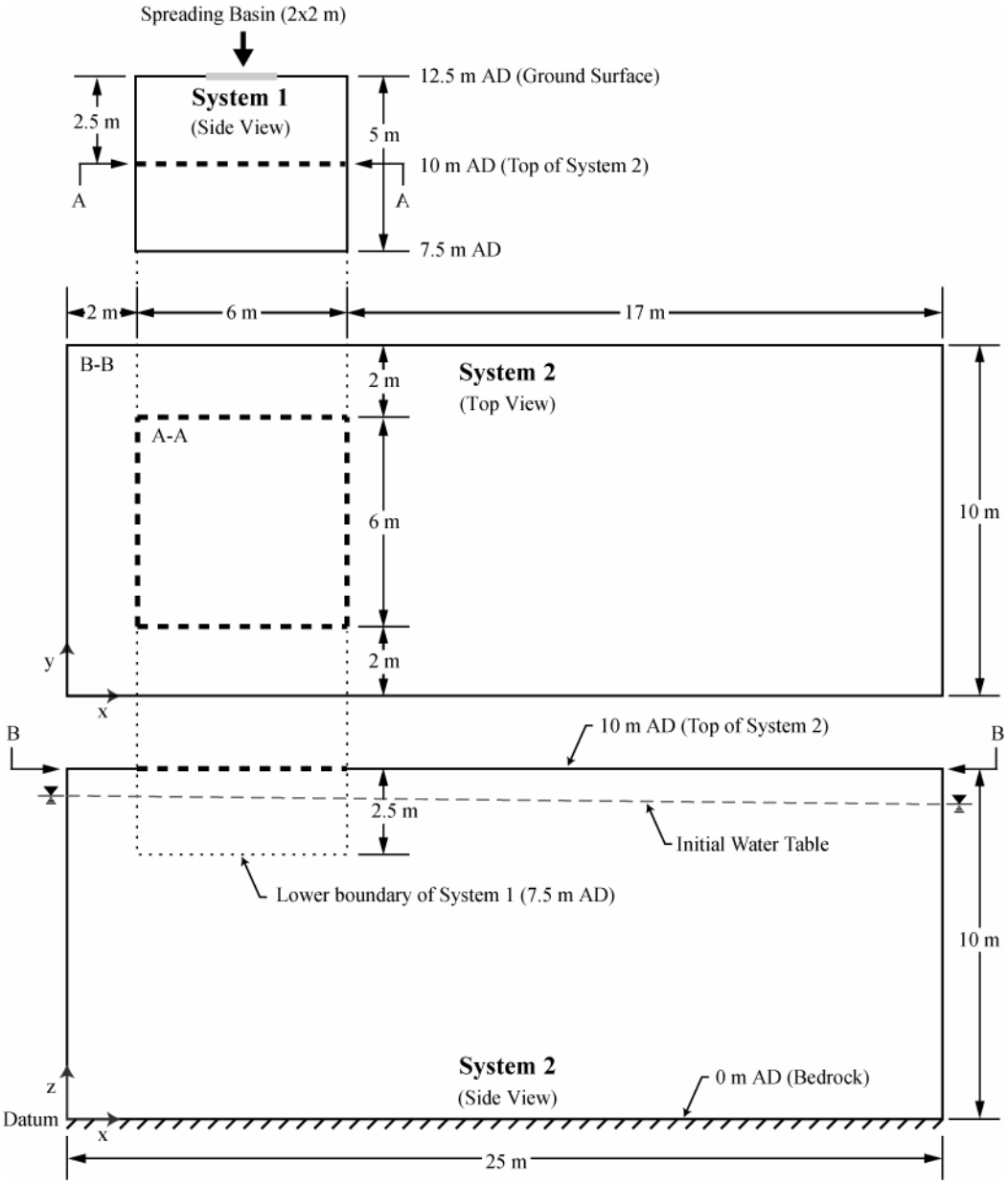

Figure 3.1: Schematic of System 1 and System 2 where AD is the distance above the datum.

3.2 Spatial Discretizations

The System 1 and System 2 finite element meshes are constructed entirely from prismatic elements (Figure 3.2). The System 1 spatial discretization (Figure 3.3) consists

of 69,589 computational nodes, N_1, forming 128,000 elements. There are one-hundred 0.05 m element layers. Any horizontal cross-section within the systems domain contains 1280 two-dimensional (2D) triangular elements. The density of 2D elements is highest beneath the 2 m by 2 m spreading basin, located at the ground surface.

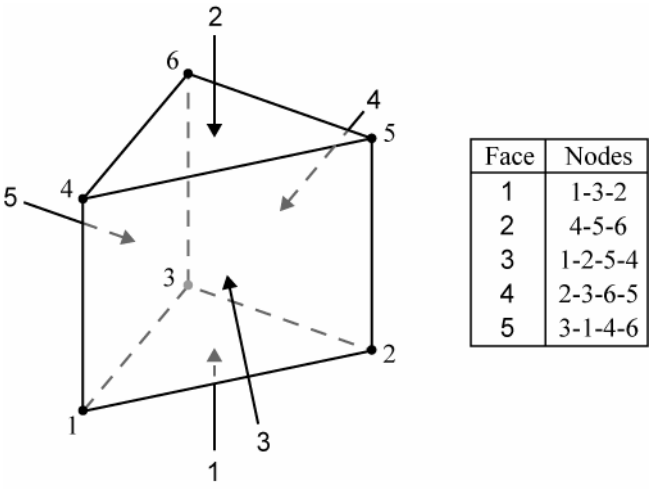

Face	Nodes
1	1-3-2
2	4-5-6
3	1-2-5-4
4	2-3-6-5
5	3-1-4-6

Figure 3.2: Prismatic element construction.

The System 2 spatial discretization (Figure 3.4) consists of 16,068 computational nodes, N_2, forming 28,576 elements. There are eighteen 0.5 m element layers between 0 m AD and 9 m AD and twenty 0.05 m element layers between 9 m AD and 10 m AD. Any horizontal cross-section contains 752 2D triangular elements. The density of 2D elements is highest beneath the spreading basin.

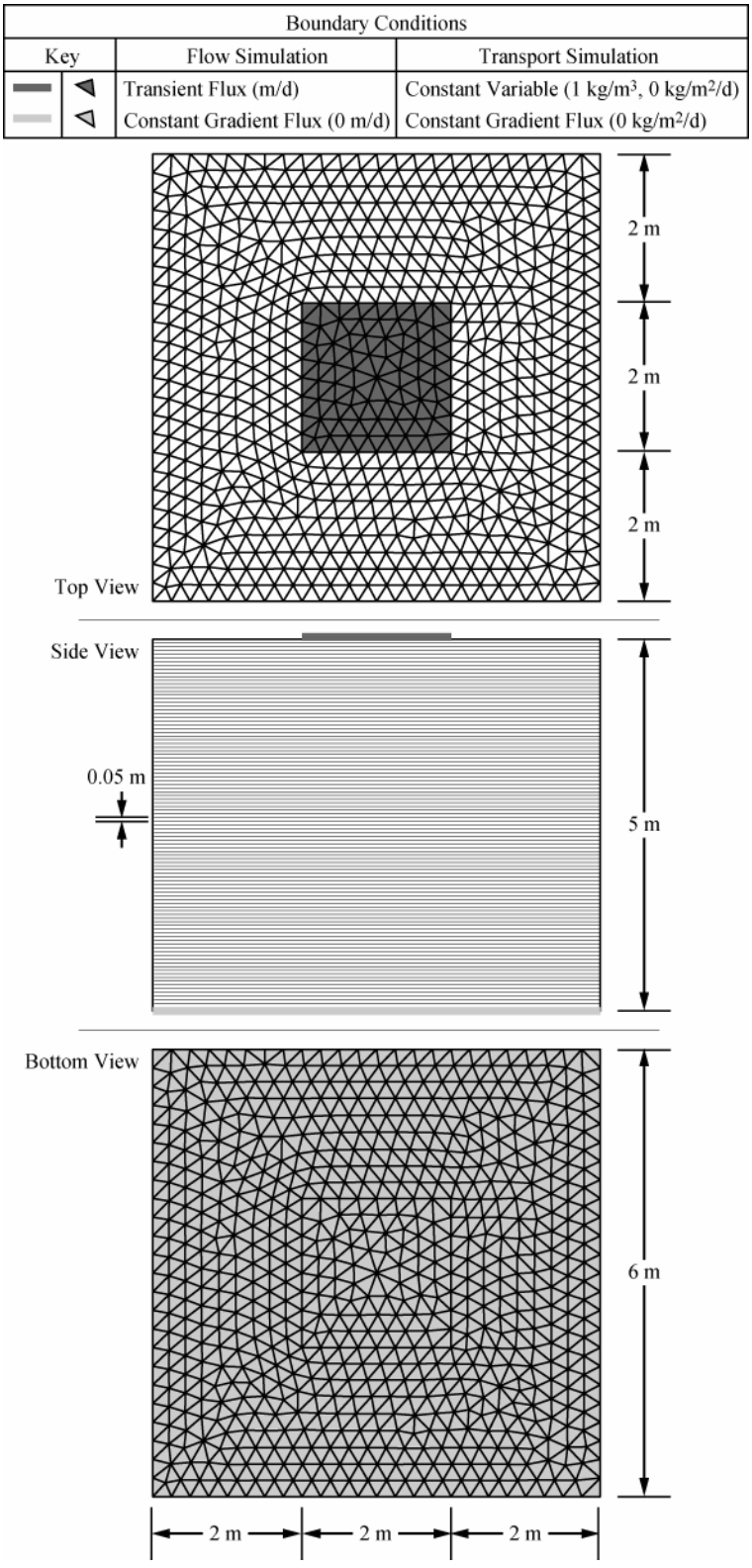

Figure 3.3: System 1 spatial discretization and boundary conditions.

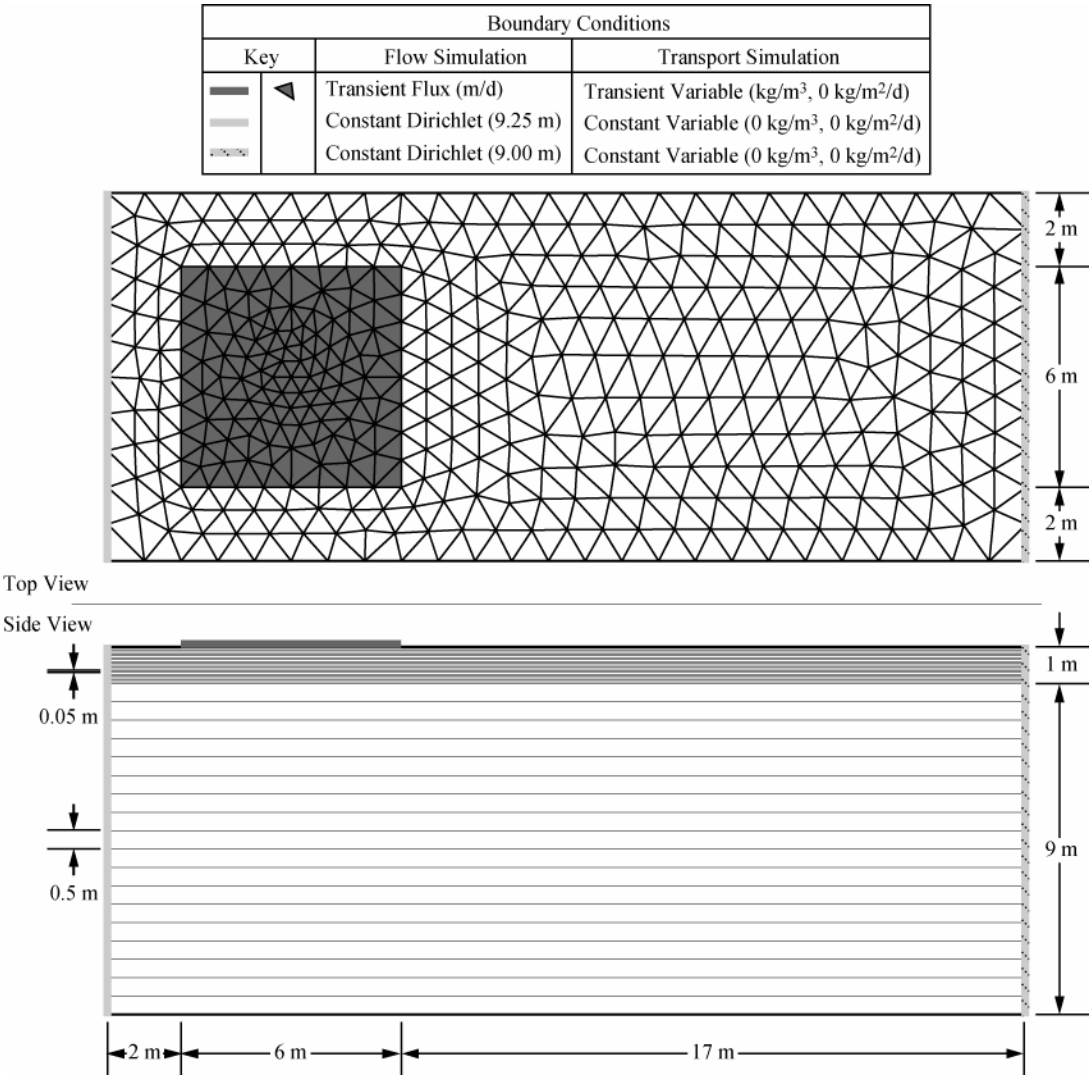

Figure 3.4: System 2 spatial discretization and boundary conditions.

3.3 Temporal Discretization

The total simulation time for System 1 is 100 days. The temporal discretization of System 1 shown in Figure 3.5 consists of twenty-thousand 0.005 day time steps. Time step size selection was based on preliminary sensitivity results for flow and transport simulations within the unsaturated zone.

The total simulation time for System 2 is 5000 days. During the first 100 days of the simulation the temporal discretization (Figure 3.5) is variable and dependent on the solution of the adaptive time step algorithm (Section 4.4). The temporal discretization for the remainder of the simulation consists of four-hundred and ninety 1 day time steps. Selection of the 1 day time step is based on preliminary sensitivity results for simulations of plume migration within the saturated zone.

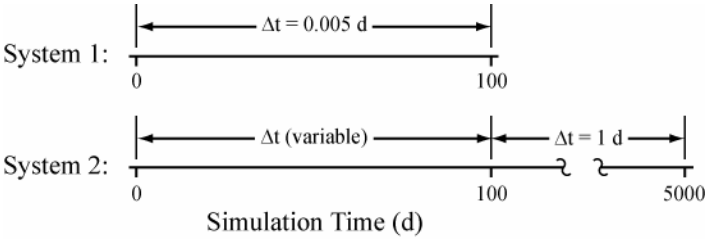

Figure 3.5: Temporal discretizations for System 1 and 2.

3.4 Boundary Conditions

The System 1 flow and transport boundary conditions are described in Figure 3.3. The system has no flow boundary conditions on the sides, a free drainage boundary condition on the bottom (McCord, 1991), and both a specified flux/concentration and no flow boundary conditions at the top (12.5 m AD). Chloride (Cl^-), a non-reactive solute, enters the system through a 2 m by 2 m spreading basin located at the ground surface. The transient infiltration rate within the spreading basin, q_r, is shown in Figure 3.6.

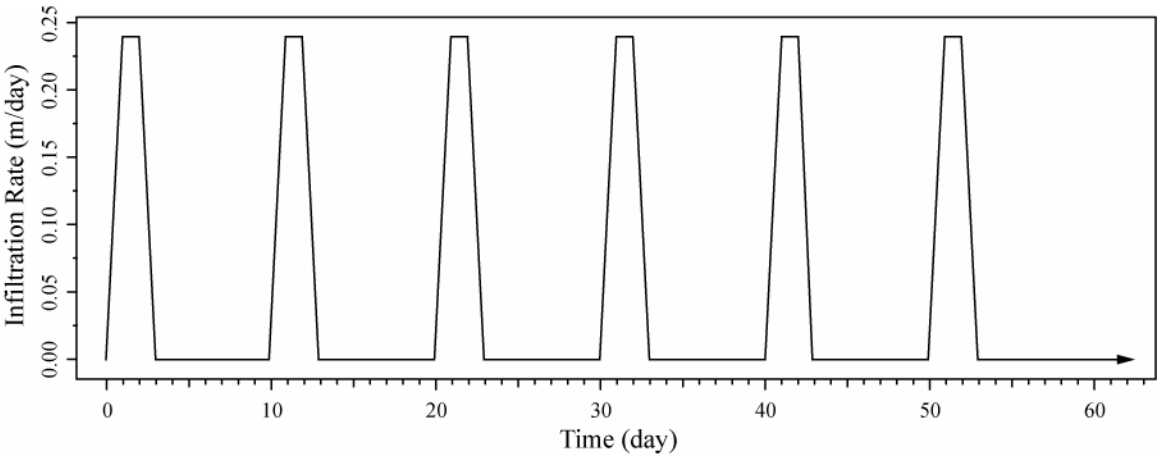

Figure 3.6: System 1 infiltration rate over time.

There are six uniform infiltration cycles occurring at ten day intervals. Each infiltration cycle is three days in duration and reaches a maximum infiltration rate, q_{max}, of 0.24 m/day. The magnitude of q_{max} is equivalent to the maximum infiltration rate implemented in the Russo et al. (2001) study. The total volume of water that infiltrates into System 1 through the ground surface is 11.52 m^3 (11,486 kg). The conservative tracer concentration of the incoming water remains constant at 1 kg/m^3.

The System 2 flow and transport boundary conditions are described in Figure 3.4. The system has no flow boundary conditions on the sides parallel to the x-axis and bottom, Dirichlet flow and variable transport boundary conditions on the sides parallel to the y-axis, and both a specified flux/concentration and no flow boundary conditions at the top (10 m AD). For the two sides parallel to the x-axis, Dirichlet flow conditions are entered as total head values, and they are converted internally by FEMWATER to pressure heads by subtracting the elevation of the nodes where the boundary conditions are assigned. The specified total head values at the two side boundaries are 9.25 m (x = 0

m) and 9.00 m (x = 25 m). The variable transport boundary condition for the two sides is dependent on the direction of flow through the boundary face. When groundwater passes into the system, through the boundary face, a Cl^- concentration of 0 kg/m^3 is specified for the incoming water. However, when groundwater exits the system through the boundary face a concentration gradient of 0 kg/m^2/day is specified, thus allowing Cl^- to exit the system with the outflowing groundwater.

3.5 Initial Conditions

Initial conditions for the numerical models are representative of a unsaturated-saturated system void of effluent infiltration. The exclusion of recharge results in a relatively dry vadose zone with moisture levels determined by the residual moisture content of the media. The initial pressure head distribution within System 1 is specified using a total head value of 4.5 m. In System 2, steady state conditions are used as the initial pressure head distribution. Where steady state reflects an unconfined aquifer undisturbed by recharge with a linear drop in the water table from an elevation of 9.25 m at x = 0 m to 9.00 m at x = 0 m. This corresponds to a hydraulic gradient of 0.01 with baseline flow moving from left to right along the x-axis. The initial Cl^- concentration for both systems is set at 0 kg/m^3.

3.6 Material Properties

Different approaches were taken to describe the soil lithology within the two systems. A high spatial variability of fluid fluxes in the vadose zone (System 1)

advocates the use of geostatistics to generate a heterogeneous soil distribution. In the unconfined aquifer (System 2), the spatial variability of fluid fluxes is assumed to be small enough to justify a homogeneous soil distribution based on average soil parameters.

The material hydraulic properties for System 1 and System 2 are described in Table 2. Five material types, identified as Soil 1, Soil 2, Soil 3, Soil 4 and Soil 5, are used to describe the single geologic realization within the vadose zone (System 1). The material types are generated from statistical distributions derived from soil data collected from the Bet Dagan trench (Russo and Bouton, 1992). The magnitude of each soil property is within one standard deviation of the mean. The unconfined aquifer (System 2) is exclusively composed of a single material type based on the mean soil properties described in Table 2.

Table 2: Material Hydraulic Properties Used in Flow Simulations.

Material	**Sat. Hydraulic Conductivity** K_s (m/day)	**Partially Saturated Flow Parameters** Θ_s	Θ_r	α (1/m)	β
Mean*	0.363	0.40	0.10	0.479	2.0
Variance*	0.91†	6E-4	4E-4	0.63†	0.04
Soil 1	0.040	0.41	0.10	1.194	2.1
Soil 2	3.265	0.40	0.12	0.191	2.0
Soil 3	1.089	0.42	0.08	0.479	1.8
Soil 4	0.121	0.38	0.11	0.077	2.2
Soil 5	0.363	0.39	0.09	2.977	1.9

* Russo et al. 2001. † Variance based on the logrithmic distribution of the parameter.

The Mualem-van Genuchten model (Equation 3.4-3.7) is used to describe the moisture retention characteristics within the vadose zone. The soil water retention curves, derived from the Mualem-van Genuchten model, are dependent on the partially saturated flow parameters in Table 2 and are shown in Figure 3.6. This empirical relationship describes the moisture content, θ_w, water capacity, $d\theta_w/d\psi$, and relative

conductivity, K_r, as a function of the capillary pressure head, ψ. Where capillary pressure head is a measure of the (positive) soil-water tension, defined as:

$$\psi = |h| \quad \text{for } h \le 0 . \tag{3.18}$$

Furthermore, the moisture content is defined as:

$$\theta_w \equiv \frac{\text{volume of water within a REV}}{\text{bulk volume of a REV}}, \tag{3.19}$$

where REV is a representative elementary volume. Taking the derivative of moisture content (Equation 3.7) with respect to capillary pressure head (Equation 3.18) gives the water capacity expressed as

$$\frac{d\theta_w}{d\psi} = \frac{\alpha \cdot (\beta - 1) \cdot (\theta_s - \theta_r) \cdot (\alpha\psi)^{\beta - 1}}{\left(1 + (\alpha\psi)^{\beta}\right)^{(2\beta - 1)/\beta}} . \tag{3.20}$$

The significance of water capacity is reflected in model convergence where sharp or extreme changes in water capacity make it more difficult for the model to converge during the iterative solution process. For example, a homogeneous system of sand would require a much finer spatial and temporal discretization than a homogeneous system of silt. In this study the peaks in water capacity for Soil 5 (characteristic of a more sand soil) push the limits of model convergence and are largely responsible for the spatial and temporal discretizations prescribed to the model.

The relative conductivity, ranging in value from 0.0 to 1.0, expresses the fraction of total hydraulic conductivity remaining when the void spaces are only partly fluid-filled and only part of the total interconnected void spaces is connected by continuous fluid channels (Lin et al., 1997). Multiplying the relative hydraulic conductivity by the

saturated hydraulic conductivity gives the effective hydraulic conductivity (Equation 3.2).

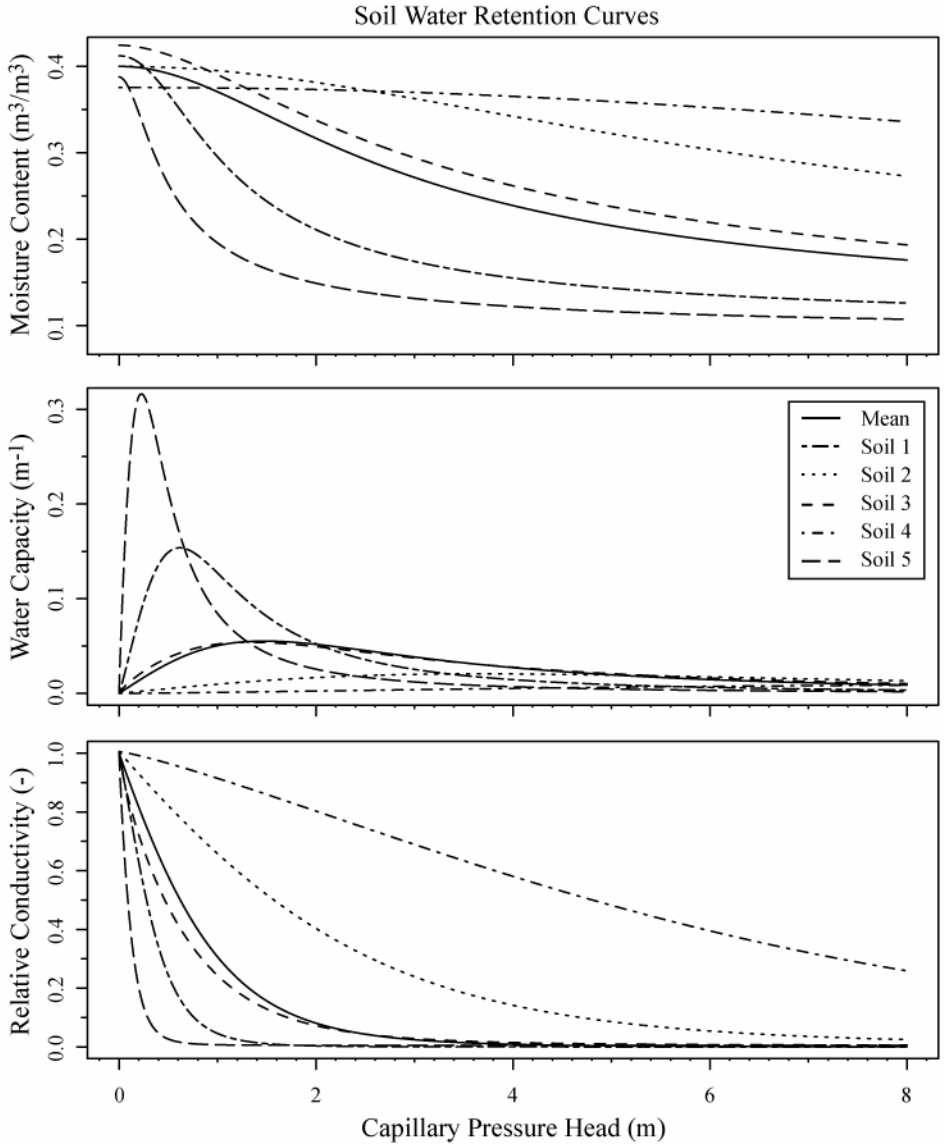

Figure 3.7: Soil water retention curves based on Equations 3.4-3.7 and soil parameters defined in Table 2.

3.7 Geospatial Distribution of Soil Properties

The System 1 heterogeneity was described using a geostatistical approach. The steps taken to generate a single realization of the subsurface lithology are presented as follows:

- Establish synthetic soil observations within the hypothetical field site. First generate random coordinate locations (x, y, z) from three uniform distributions, each distribution corresponding with a principle axis. The upper and lower limits of the distributions are dictated by the spatial dimensions of the field site. The total number of synthetic observations used in this study is 100.
- Associate with each of the coordinate locations, k, a random number, $\hat{u}_k$, generated from a normal distribution with a mean of zero and a standard deviation of one. These numbers are the observed data that will later be transformed into soil types.
- Construct a block mesh within the systems spatial domain. Not unlike the total number of synthetic observations used, the resolution of the block mesh will ultimately affect the spatial variations in the subsurface lithology. The mesh implemented here contains 189,771 nodes forming 180,000 block elements where each block side is 0.1 m in length.
- Develop variogram models in the horizontal and vertical dimensions using Gstat (Pebesma, 1998). The synthetic variogram models used in this study are shown in Figure 3.7 and were constructed using an anisotropy ratio (vertical/horizontal) of 0.1, exponential model type, sill of 0.22, range of 2.74 and a nugget of 0 (McCord, 1997).

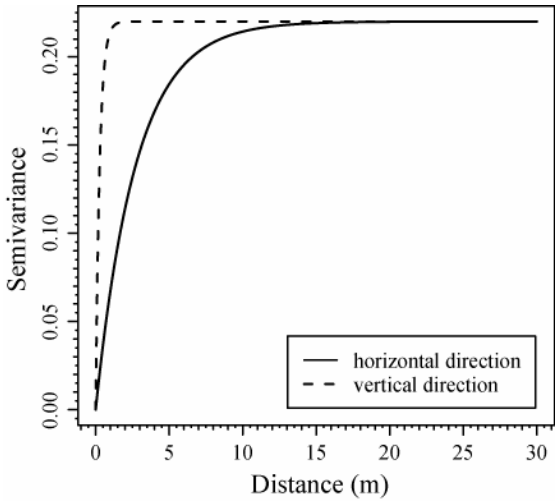

Figure 3.8: Variogram models in the horizontal and vertical directions.

- Estimate a numeric value, u_j, for each node, j, within the block mesh using the ordinary point kriging algorithm implemented in Gstat. The algorithms input requirements include the block mesh, synthetic soil observations and variogram models.
- For each node, transform u_j into a soil type, s_j. The soil types used in this study are identified as Soil 1 (s = 1), Soil 2 (s = 2), Soil 3 (s = 3) , Soil 4 (s = 4) and Soil 5 (s = 5). First, define cutoff values, v_c, within the domain of u. The number of unique cutoff values, N, is equal to the total number of soil types plus one and includes both the minimum and maximum values of u. Soil values lying between two adjacent cutoff values are then identified as belonging to a particular soil type. The soil type identification process is made using indicator variables, i_j, defined as

$$i_j\left(v_c, v_{c+1}\right) = \begin{cases} 1 & \text{if } v_c < u_j \le v_{c+1} \\ 0 & \text{otherwise.} \end{cases} \tag{3.21}$$

The cumulative proportion of values between sequential cutoffs can then be expressed as

$$F\left(v_c, v_{c+1}\right) = \frac{1}{n}\sum_{j=1}^{n} i_j\left(v_c, v_{c+1}\right) \tag{3.22}$$

where F is equivalent to the proportion of a given soil type within the system. By manipulating the inner cutoff values, v_2 through v_{N-1}, it is then possible to change the proportion of each soil type within the system. If the true soil type proportions, P_c, are known/estimated in advance (e.g. from borehole logs), then the inner cutoff values may be identified by minimizing the squared differences between the calculated and true soil type proportions by varying the inner cutoff values. The optimization (integer-programming problem) is expressed as

$$\min_{v_2, v_3, \ldots, v_{N-1}} \sum_{c=1}^{N-1}\left(F\left(v_c, v_{c+1}\right) - P_c\right)^2 \tag{3.23}$$

and solved using a genetic algorithm (Carroll, 2001). For this study the true proportion of Soil 1 (P_1), Soil 2 (P_2), Soil 3 (P_3), Soil 4 (P_4) and Soil 5 (P_5) are equivalent at 20%. Using the set of optimal cutoff values the soil type, s_j, is identified for each node in the block mesh.

- Determine the soil values, $\tilde{u}_m$, at each node, m, in the finite element mesh of System 1 using linear basis functions.
- Finally, determine the soil type, s_e, for each prismatic element, e, in the System 1 finite element mesh by averaging an elements nodal soil values and rounding to the nearest integer value. The calculation is expressed as

$$s_e \approx \frac{\sum_{i=1}^{6} \tilde{u}_{m_{e,i}}}{6} \quad \text{(round), for } e = 1, \ldots, E \tag{3.24}$$

where $m_{e,i}$ is the node associated with the i^{th} node in element e. The resulting synthetic lithology for System 1 is shown in Figure 3.8.

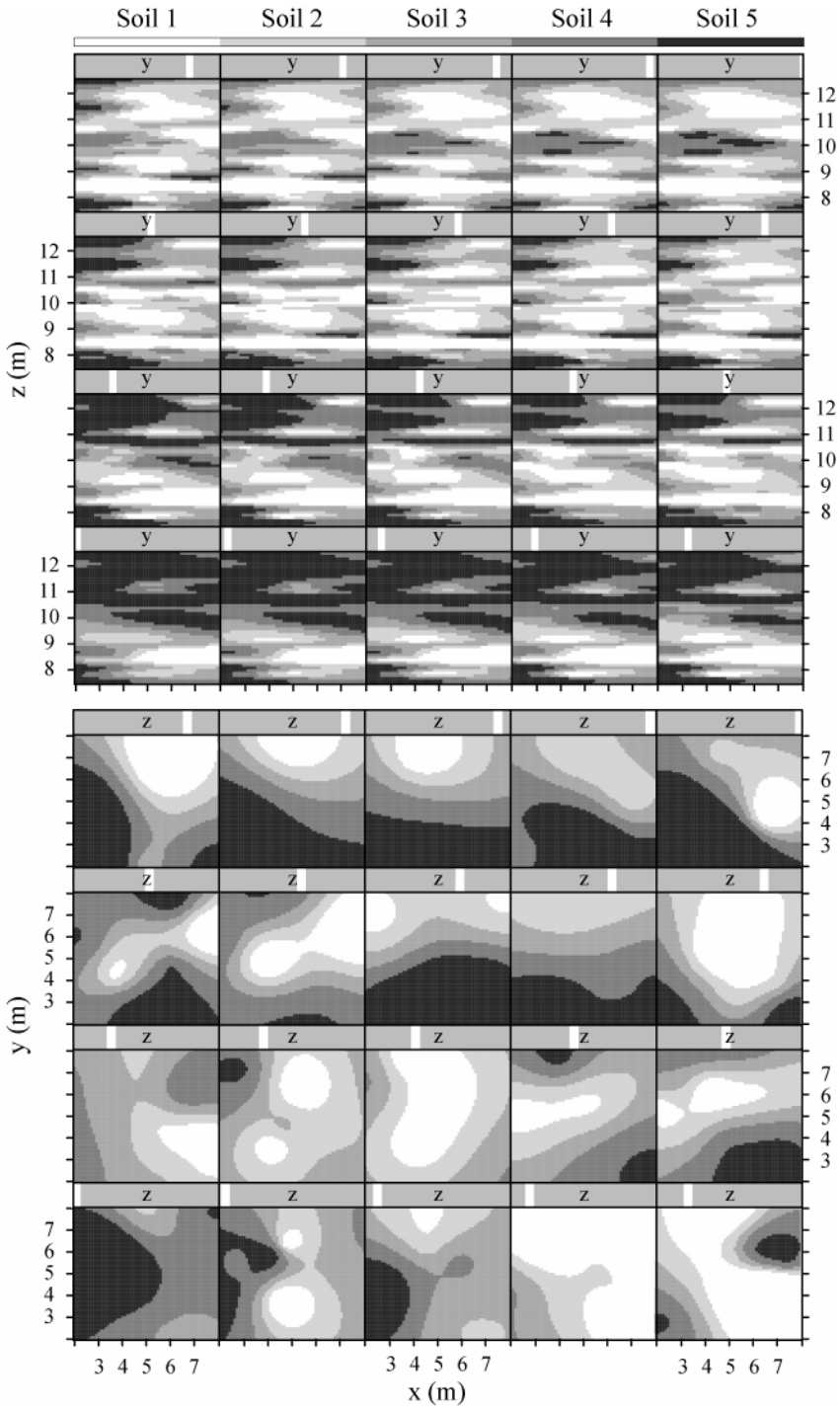

Figure 3.9: The System 1 synthetic media realization (not to scale). The 3D media distribution is visualized using 2D cross-sections. There are 20 vertical (x-z plane) cross-sections and 20 horizontal (x-y plane) cross-sections.

3.8 Computer Hardware and Software

A brief summary is made of the computer hardware and software used in this dissertational research. The computer hardware included two Intel Pentium IV class computers, each with 1 GB of RDRAM memory and 160 GB of disk space. The software configurations for the two computers were identical with applications running on a Microsoft Windows XP Professional operating system (Service Pack 2). Compaq Visual Fortran Professional 6.6 was used to compile the Fortran FEMWATER 3.0 source code. Finite element mesh construction and pre-processing of the FEMWATER input files was done using GMS 4.0. The post processing and analysis of the FEWATER output was carried out using GWplot 0.2. Supporting software for GWplot includes R 2.0 (Ihaka et al., 1996), a language and environment for statistical computing and graphics, and MySQL 4.0, a database server.

4 RECHARGE BOUNDARY CONSTRUCTION

An algorithm is presented for the construction of a recharge boundary within System 2 using pressure head and concentration distributions calculated from a System 1 simulation. Throughout the description of the algorithm (Chapter 4) references to System 1 and System 2 may be defined in general terms as any two 3D finite element models where, (a) System 1 spatially intersects with System 2, (b) a portion of the spatial domain of System 1 lies above the spatial domain of System 2, and (c) that the horizontal spatial domain (x-y plane) of System 1 is completely contained within the horizontal spatial domain of System 2. Data requirements for the algorithm include the model geometry of

System 1 and System 2 as well as the pressure heads and concentrations determined from a System 1 simulation. The algorithms output, the recharge boundary condition for System 2, is the transient fluid fluxes and concentrations associated with those element faces within the upper boundary of System 2 that are contained within the spatial region described by the intersection of System 1 and System 2.

To accommodate for differing spatial discretizations for the two systems (Figure 4.1), the algorithm relies upon underlying properties of a finite element approach. The first of these properties constrains the geometric shape of all element faces as planer triangles with minimum interior angles. The second property is the ability to calculate a state variable at any given coordinate location within the system. For example, given output from a System 1 simulation, the pressure head and concentration may be calculated at any point (x, y, z) in the system for all time steps. The usefulness of these properties is better understood with a more detailed explanation of the algorithm. The following sections present the solution steps required to determine the System 2 recharge boundary condition. Sections 4.1, 4.2 and 4.3 address the mass flux calculation for a single triangular element and Sections 4.4 and 4.5 demonstrate techniques for resolving time step differences between System 1 and System 2.

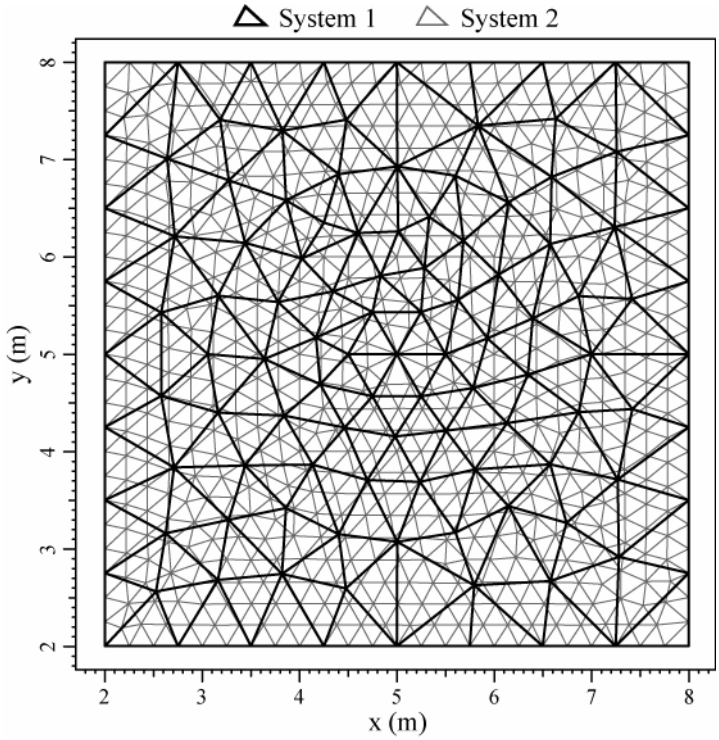

Figure 4.1: Mesh overlap for System 1 and System 2.

4.1 Adaptive Spatial Mesh

Differences between the spatial discretization of System 1 and System 2 are typically due to a much finer spatial resolution within System 1. An adaptive spatial mesh is used to capture the higher resolution of System 1 within the System 2 recharge boundary. The first requirement for implementing the adaptive spatial mesh routine within a single boundary element face is the generation of a sequence of 2D finite element meshes. Every mesh within the sequence shares a common spatial domain. Mesh placement within the sequence is a function of the mesh's spatial resolution. This functional relationship between the level of resolution, i, and the total number of elements in the mesh, e_i, is expressed as

$$e_i = 4^{i-1}, \quad i = 1, \ldots, i_{max} \tag{4.1}$$

where i_{max} is a user defined maximum resolution level. For example, setting $i_{max} = 3$ results in three separate meshes corresponding to three levels of resolution. The first of these meshes, $i = 1$, contains a single element, the dimensions of which are identical to the original recharge element face of System 2.

Mesh construction for levels of resolution greater than one use as their template the mesh constructed from the previous level of resolution. Figure 4.2 shows the node and element indexing for a sequence of meshes corresponding to the first three levels of resolution. The indexing for nodes of identical spatial placement is constant in order to relate the meshes as resolution increases. For example, the spatial locations of nodes 1, 2, and 3 remain constant for all three meshes.

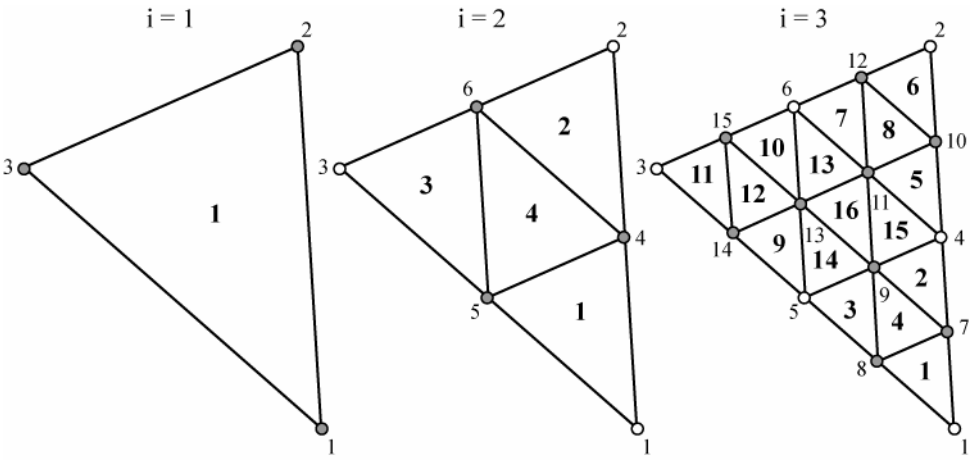

Figure 4.2: Node and element indexing for mesh generation. Closed circles indicate nodes that have been added to the spatial mesh in resolution level i.

The methodology for mesh refinement going from i to i + 1 is as follows: (a) Select the first element in mesh i. (b) Calculate the midpoints for line segments formed

when connecting the element vertices, P. Where, M_1, M_2, and M_3 are the respective midpoints for line segments connecting P_2 to P_3, P_3 to P_1 and P_1 to P_2. (c) Construct new elements in mesh i + 1 using the mesh template in Figure 4.3.

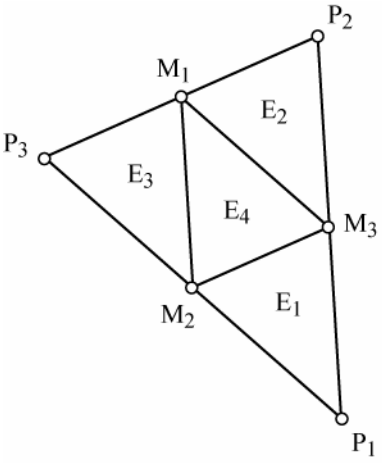

Element	Vertices		
E_1	P_1	M_3	M_2
E_2	M_3	P_2	M_1
E_3	M_2	M_1	P_3
E_4	M_1	M_2	M_3

Figure 4.3: Element template for mesh construction.

(d) Identify the element numbers for the newly created elements. There are four elements produced from the refinement of a single element. (e) Step through each of the newly formed elements assigning node numbers to those points not already identified as nodes. Node and element indexing is based upon the template shown in Figure 4.3. (f) Store the element and nodal information for later use and repeat the procedure for every element in the mesh.

4.2 Flow and Transport Calculations

Calculation of the flow and transport through a single System 2 recharge boundary element face requires both a multiple resolution mesh (Section 4.1) and the ability to determine the pressure head and concentration at any point within System 1.

The mathematical formulation for the calculation of a state variable within the systems domain is excluded from this dissertation due to the reliance of the formulation on the specific type of basis functions used within the 3D finite element model. The general concept behind the formulation is, however, presented in most introductory finite element books (Pinder et al., 1977; Lapidus et al., 1982).

The ability to determine h and C at (x, y, z) allows for the calculation of fluid flux and solute transport through any 2D element within the System 1 spatial domain (Figure 4.4). Darcy's Law gives the vertical fluid flux (a.k.a. specific discharge) through a partially saturated medium, q_c, as

$$q_c = K_{s,z} K_r\left(h_c\right) \cdot \left(\frac{h_{1,c} - h_{2,c}}{\Delta z} + 1 \right) \quad \text{for } c = 1, \ldots, T_1 \tag{4.2}$$

where c is the time step index for System 1, T_1 is the total number of time steps in the System 1 simulation, and h_1 and h_2 are the pressure heads at a distance of $\Delta z/2$ above and below the centroid of the element, respectively. The magnitude of Δz is user-defined. The sensitivity of the RBCA to changes in Δz is examined in Section 5.2. The values of K_s and K_r are determined by identifying the soil type of the System 1 element containing point (x, y, z). It is important to note that Equation 4.2 only describes vertical flow through the element with horizontal flow assumed negligible. The equation could, however, be reformulated to accommodate for flow in multiple directions.

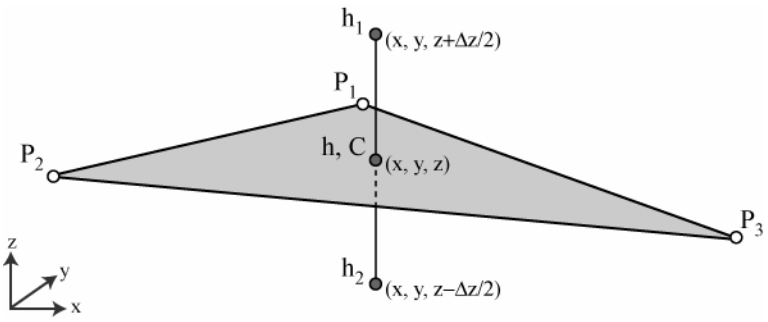

Figure 4.4: Pressure head gradient calculation.

The fluid mass passing through the element during a single System 1 time step is defined as

$$m_c = q_c \rho A_e \cdot \left(t_{1,c} - t_{1,c-1} \right) \quad \text{for } c = 1, \ldots, T_1 \tag{4.3}$$

where $t_{1,c-1}$ and $t_{1,c}$ are the respective start and end times for time step c and A_e is the elements area. Summing m_c over all time steps in the simulation gives the total liquid mass, M, expressed as

$$M = \sum_{c=1}^{T_1} m_c \tag{4.4}$$

The constituent mass, $\tilde{m}_c$, passing through the element during a single System 1 time step is defined as

$$\tilde{m}_c = q_c C A_e \cdot \left(t_{1,c} - t_{1,c-1} \right) \quad \text{for } c = 1, \ldots, T_1 \tag{4.5}$$

where C is the concentration at the elements centroid for the end of time step c.

Mass values are then initialized as multi-dimensional arrays linking m_c, M, and $\tilde{m}_c$ to the multiple resolution mesh. The mass arrays are expressed as $m_{c,\,i,\,j,\,k}$, $M_{i,\,j,\,k}$, and $\tilde{m}_{c,\,i,\,j,\,k}$ where i is the current resolution level, j is the element index for the current

resolution level, and k is an array of stored element indices for all resolution levels. Figure 4.5 gives the M indexing (i, j, k) within three resolution levels. The translation between array indexes and element numbers, e, is defined as

$$\begin{aligned} \hat{e}_1 &= 1 \\ \hat{e}_f &= 4\hat{e}_{f-1} - 4 + k_f \quad \text{for } f = 2,\ldots,i \\ e &= \hat{e}_i \end{aligned} \tag{4.6}$$

where $\hat{e}$ is a temporary single array. For example, if i = 3 and k = (1, 2, 4) than the calculation of e is expressed as

$$\begin{aligned} \hat{e}_1 &= 1 \\ \hat{e}_2 &= 4\hat{e}_1 - 4 + k_2 = 4 \cdot 1 - 4 + 2 = 2 \\ \hat{e}_3 &= 4\hat{e}_2 - 4 + k_3 = 4 \cdot 2 - 4 + 4 = 8 \\ e &= \hat{e}_3 = 8. \end{aligned} \tag{4.7}$$

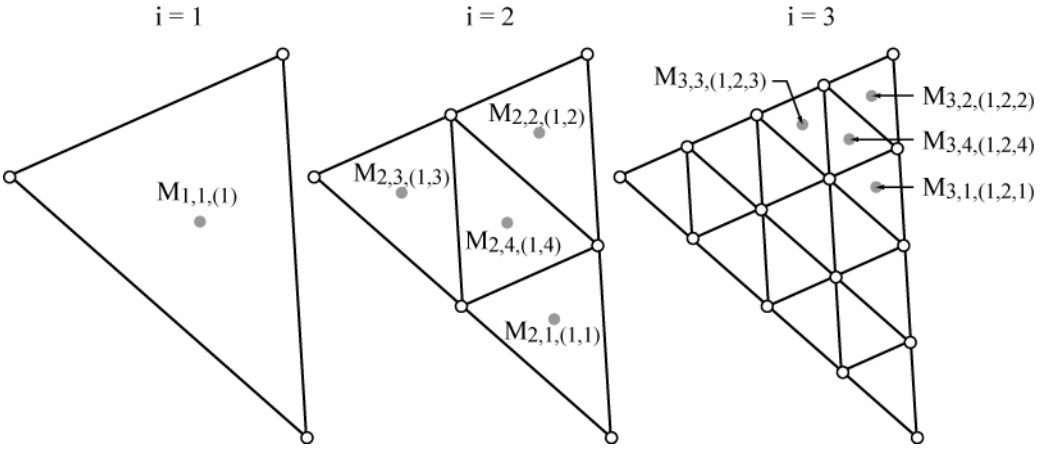

Figure 4.5: Total fluid mass indexing for three levels of resolution, $M_{i,j,k}$.

4.3 Mass Search

A mass search algorithm, based on a mass balance approach, is used to calculate the mass moving through a single System 2 recharge boundary element face. A

flowchart for the algorithm is given in Figure 4.6. The premise for the algorithm is the collection of state variable information within System 1 at a level of resolution controlled by the user. The user defined input parameters (a.k.a. control parameters) are: (a) TOL, the maximum percent difference in total mass between two resolution levels. The percent difference is calculated for every iteration of the mesh refinement process and defined as

$$\frac{\left|M_{i,j,k_i} - M_{sum}\right|}{0.5\left(M_{i,j,k_i} + M_{sum}\right)}\ 100 \tag{4.8}$$

where

$$M_{sum} = \sum_{j=1}^{4} M_{i+1,j,k_{i+1}}\ . \tag{4.9}$$

If the percent difference is less than TOL, the search moves to a higher resolution level, otherwise, the refinement process halts. (b) i_{max}, the maximum resolution level, an upper limit on the number of possible mesh refinements. (c) M_{low}, a lower mass limit on M_{sum}. If M_{sum} is less than M_{low} the refinement process is halted.

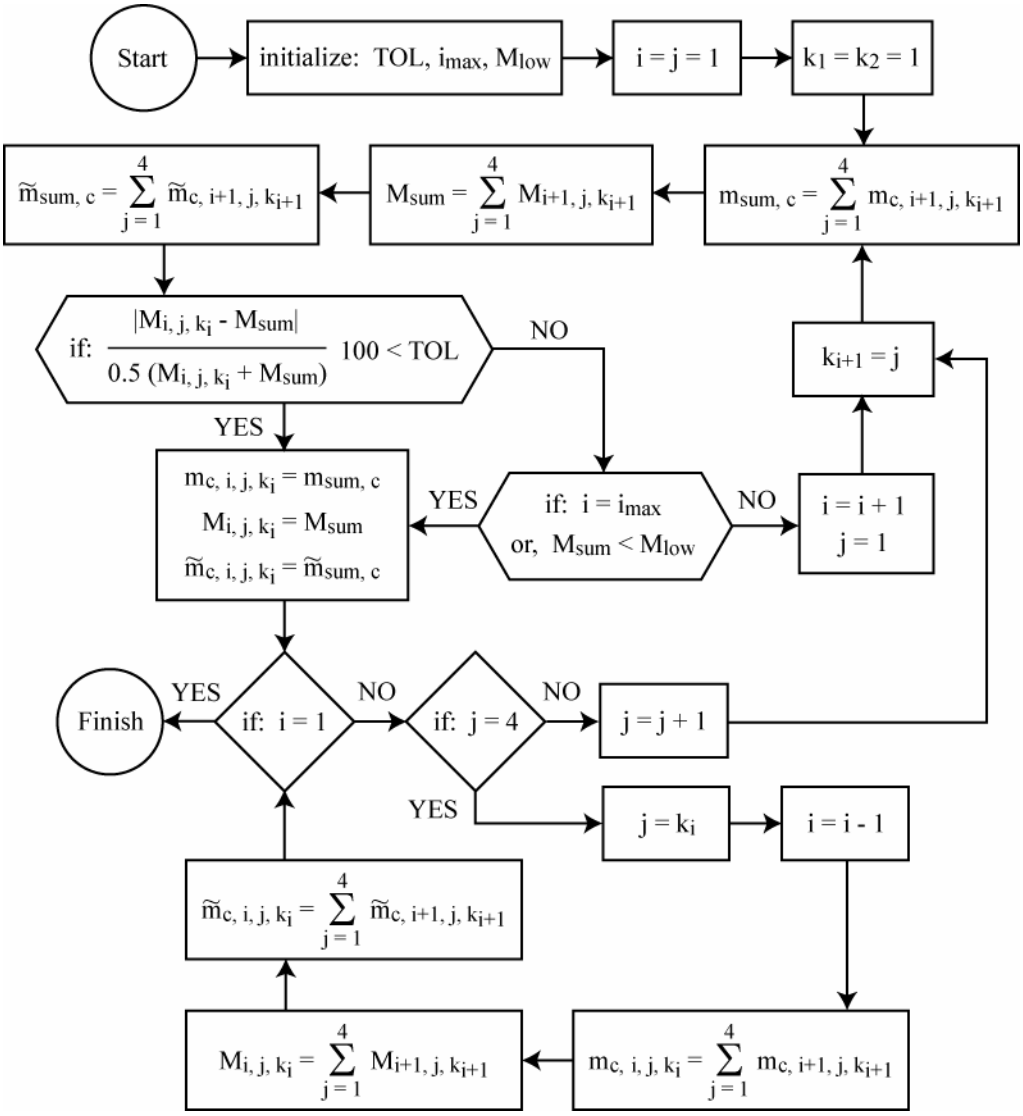

Figure 4.6: Flowchart for Adaptive Spatial Mesh Algorithm.

4.4 Adaptive Time Steps

After calculating the mass passing through each of the triangular element faces at every System 1 time step, an adaptive time step algorithm is implemented to determine the recharge timing for System 2. The System 2 recharge time steps, t'_2, are determined from a simplification of the System 1 temporal discretization. For example, an increase

in the temporal step size is made during periods of minimal flow through the CP or during periods when the rate of change in fluid flow varies insignificantly. The advantages to simplifying the temporal discretization are two-fold. First, fewer points are necessary to describe the recharge boundary condition within System 2, thus reducing the computational burden on the numerical simulation. Second, the simplified time series may be used as a template for the System 2 temporal discretization during periods of recharge.

The user-defined input parameters for the adaptive time step algorithm control the level of temporal resolution within the System 2 recharge boundary condition. The first input parameter, m_{low}, is the lower mass limit on the maximum allowable mass that can enter System 2 through the recharge boundary during a single time step. The second input parameter, tol, is the maximum percent difference between cumulative total mass values at sequential System 2 recharge times. A flowchart for the adaptive time step algorithm is provided in Figure 4.7.

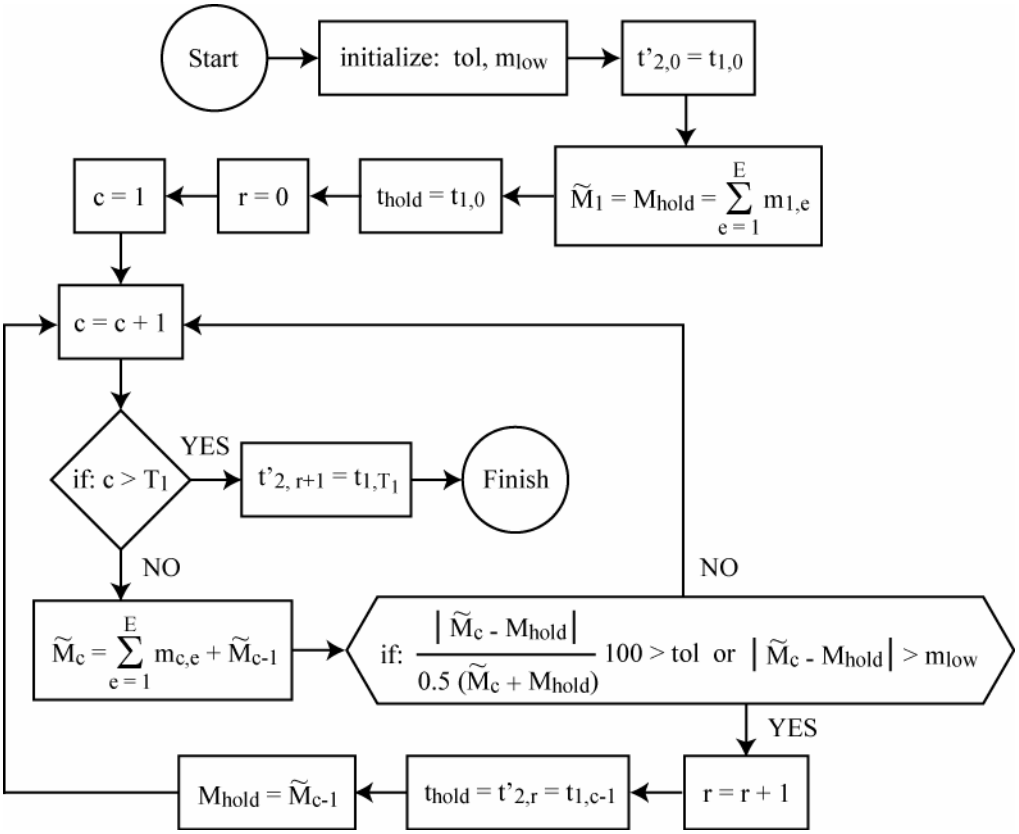

Figure 4.7: Flowchart for Adaptive Time Step Algorithm.

4.5 Temporal Transformation

To reconcile the time step differences between System 1 and System 2 requires a temporal transformation of the masses. Mass values are first summed over the System 2 time steps assuming a finer temporal discretization within System 1. A flow chart for the temporal transformation between System 1 and System 2 is given in Figure 4.8, where d is the time step index for System 2, T_2 is the total number of time steps in the System 2 simulation, $t_{2,d-1}$ and $t_{2,d}$ are the respective start and end times for time step d, and m'_d is the mass of the fluid passing through the element during time period d. The constituent

mass passing through the element during time period d, $\tilde{m}'_d$, is determined using the same methodology outlined for m'_d.

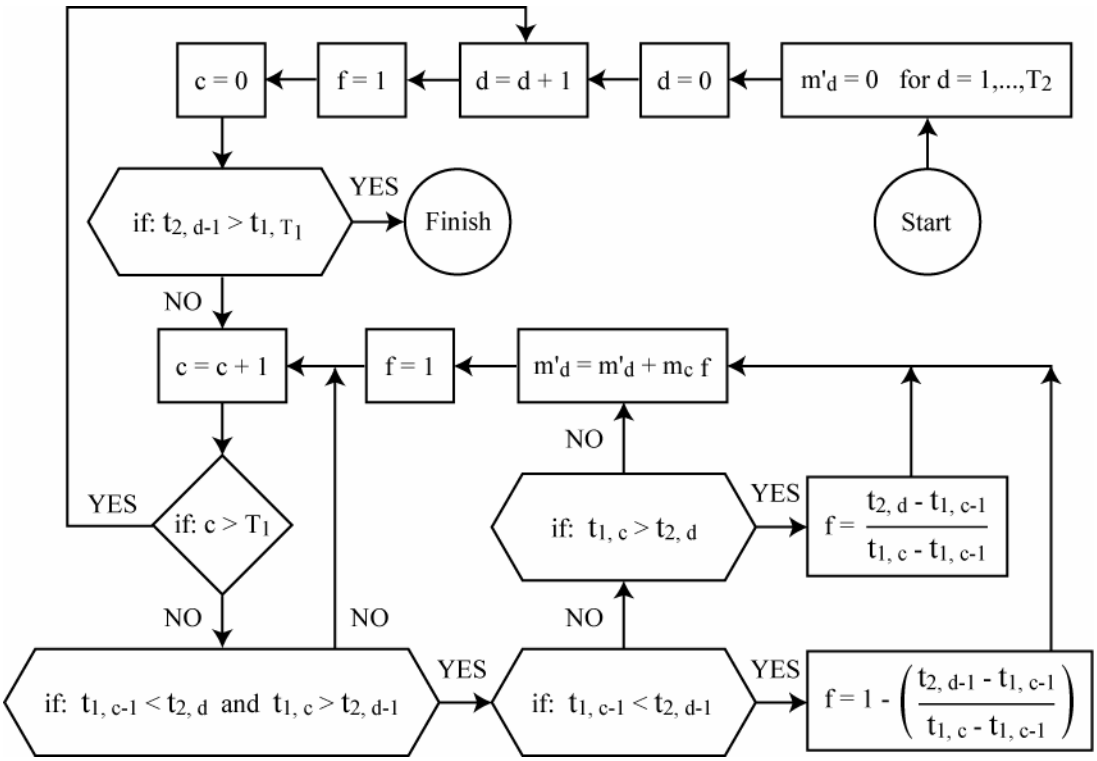

Figure 4.8: Temporal transformation flow chart for reconciling time step differences between the unsaturated (System 1) and saturated (System 2) simulations.

An example is presented to illustrate the temporal transformation from System 1 to System 2. The fluid mass passing through an element during a single System 2 time step is determined for the hypothetical temporal discretizations described in Figure 4.9. The mass calculation for time step 2 of System 2 is expressed as

$$m'_2 = m_3\left[1-\left(\frac{t_{2,1}-t_{1,2}}{t_{1,3}-t_{1,2}}\right)\right] + m_4 + m_5\cdot\left(\frac{t_{2,2}-t_{1,4}}{t_{1,5}-t_{1,4}}\right) \qquad (4.10)$$

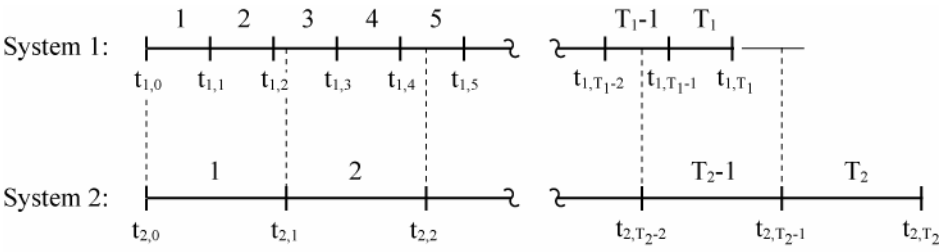

Figure 4.9: Example temporal discretizations for System 1 and System 2.

After the temporal transformation the fluid mass, m'_d, is converted back to a fluid flux, q, using

$$q_d = \frac{m'_d}{\rho \cdot \left(t_{2,d} - t_{2,d-1}\right) A_e} \quad \text{for } d = 1, \ldots, T_2 \tag{4.11}$$

where ρ is the density of water at 25 ˚C (997.075 kg/m^3) and A_e is the area of the System 2 recharge boundary element face. In addition, the constituent mass, $\tilde{m}'_d$, is converted to a concentration, C, using

$$C_d = \frac{\tilde{m}'_d}{q_d \cdot \left(t_{2,d} - t_{2,d-1}\right) A_e} \quad \text{for } d = 1, \ldots, T_2 \tag{4.12}$$

5 RESULTS

Results are first presented for a System 1 homogeneous flow simulation (Section 5.1). A mass balance validation of the RBCA is made along with an analysis of the sensitivity of the RBCA to changes in the vertical (z-axis) position of the System 1 lower boundary. Results are then given for a System 1 heterogeneous flow and transport simulation (Section 5.2). A comparison is made between the homogeneous and heterogeneous simulations followed by a sensitivity analysis of the RBCA to changes in

the algorithms control parameters. Finally, results are presented for a System 2 flow and transport simulation based on the output of a System 1 heterogeneous flow and transport simulation (Section 5.3). Unless otherwise stated, the RBCA was run using base-case control parameters: (a) a maximum resolution level, i_{max}, of 3, (b) a maximum percent difference, TOL, of 5 %, (c) a lower mass limit, M_{low}, of 5 kg and (d) a spatial step size, Δz, of 0.05 m.

5.1 System 1 Homogeneous Flow Simulation

Validation of the numerical model and the RBCA is hindered by the complexity of partially saturated flow and transport within a 3D heterogeneous groundwater environment. Therefore, to aid in the validation process, the numerical model is simplified to a homogeneous flow simulation. Results from the simplified simulation are shown in Figure 5.1. Vertical profiles (y = 5 m) of the capillary pressure head distribution are shown after 1, 10, 25, 51, 65 and 100 days of simulation. As expected, each of the distributions exhibits a symmetric flow pattern characteristic of groundwater movement under homogeneous conditions. Water enters the system through the spreading basin (z = 12.5 m), percolates downward via gravity drainage and capillary suction, and exits the system through the lower horizontal boundary (z = 7.5 m). The cyclic nature of infiltration (Figure 3.6) in the system is clearly shown within the capillary pressure head distributions. For example, the capillary pressure heads after 51 days of simulation describe the sequential movement of two distinct water pulses. Once infiltration has ceased (t = 53 d), a period of drainage begins. The pattern of drainage is

described within the capillary pressure head distributions after 65 and 100 days of simulation.

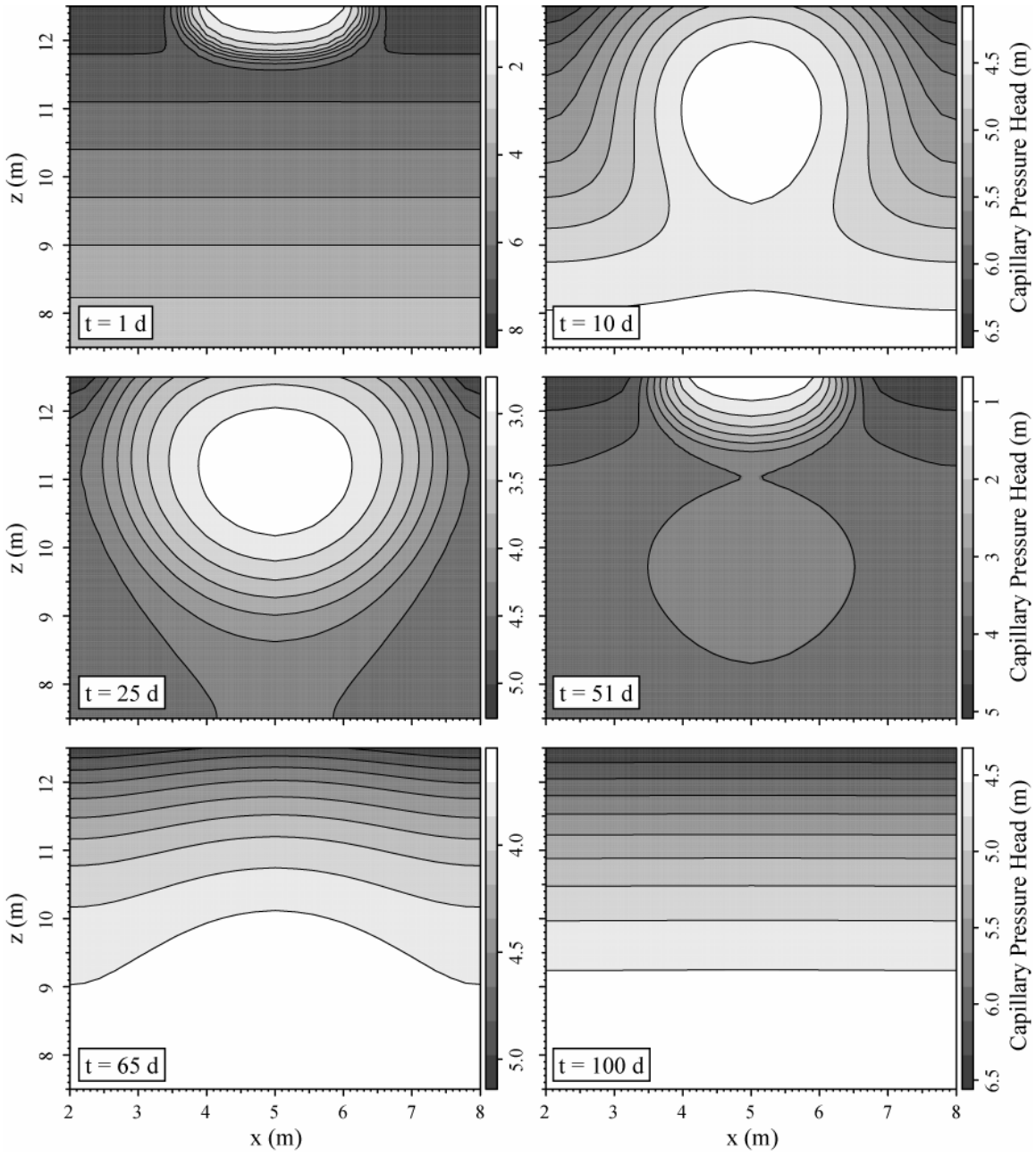

Figure 5.1: The capillary pressure head distributions within a vertical cross-section (y = 5 m) of a homogeneous realization of System 1 after 1, 10, 25, 51, 65 and 100 days of simulation.

Figure 5.2 displays the capillary pressure head distribution within the CP (z = 10 m) after 10, 51 and 100 days of simulation. Accompanying each of the capillary pressure head distributions is the fluid flux distribution for identical simulation times. Where fluid fluxes are calculated by the RBCA using the System 1 homogeneous pressure heads. As expected, the distribution patterns of capillary pressure heads and fluid fluxes are identical. For example, after 10 days of simulation the initial pulse of water introduced to the system during the first infiltration cycle has percolated downward and passed partially through the CP (Figure 5.1). The conically shaped wetting front of the water pulse is characterized in the bell shaped distribution of capillary pressure heads within the CP. Under these flow conditions one would expect to see the high fluid fluxes in areas of low capillary pressure head (high moisture content).

An analysis of the fluid flux distributions over time shows a change in fluid flux coinciding with the schedule of infiltration (Figure 3.6). The average fluid flux value after 10, 50 and 100 days of simulation is 0.0012 m/d, 0.0067 m/d and 0.0010 m/d, respectively. The increase in fluid flux going from day 10 to day 51 is due to the multiple infiltration cycles during the first half of the simulation. The relatively small fluid flux's of day 100 reflects the state of the system after 47 days of drainage with no infiltration.

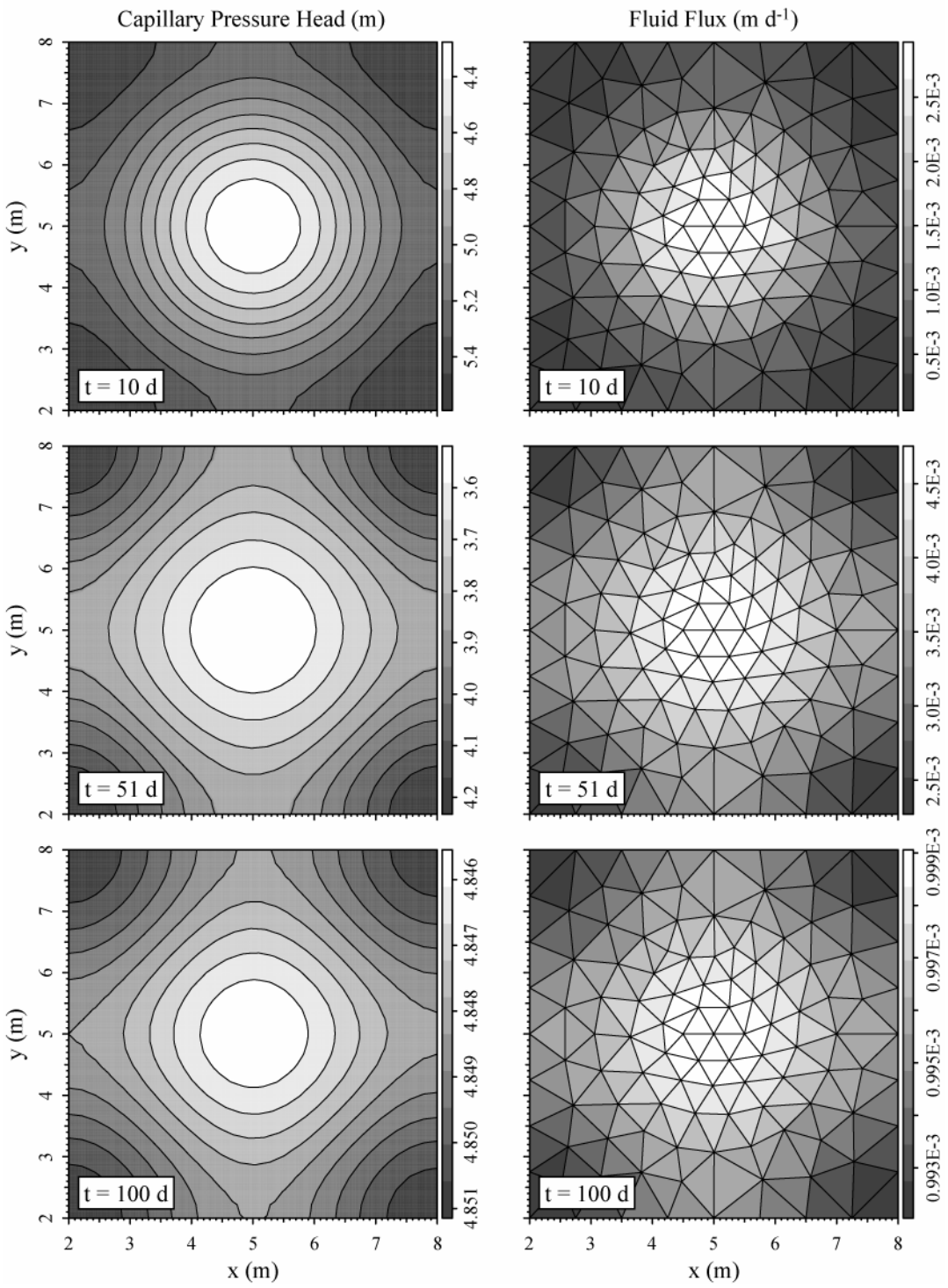

Figure 5.2: The capillary pressure head and fluid flux distributions within a horizontal cross-section (z = 10 m) of a homogeneous realization of System 1 after 10, 51 and 100 days of simulation.

A mass balance approach for validating the RBCA is shown in Figure 5.3. An estimate of the cumulative mass passing through the CP (A) is determined by subtracting the change in mass storage for water above the CP (B) from the cumulative mass of water infiltrating into the system from the ground surface (C). Mass storage, ΔS, is defined as

$$\Delta S(t) = \sum_{i=1}^{N} \begin{cases} \Theta_w\left(\hat{h}_i(t), \Theta_s, \Theta_r, \alpha, \beta\right) \forall_i \rho & \text{if } z_{min,i} \geq z_{cp} \\ 0 & \text{otherwise.} \end{cases} \quad (5.1)$$

where N is the total number of elements in System 1, $\forall_i$ is the volume of element i, $z_{min,i}$ is the minimum elevation for all nodes within element i, z_{cp} is the elevation of the CP and $\hat{h}_i$ is the average hydraulic head expressed as

$$\hat{h}_i(t) = \frac{\sum_{j=1}^{6} h_{i,j}(t)}{6} \quad \text{for element i.} \quad (5.2)$$

Validation of the RBCA is accomplished by comparing the cumulative mass passing through the CP calculated by the mass balance approach (A) and the RBCA (D).

The accuracy of the RBCA is quantified using the percent difference between total cumulative mass values. Assuming the mass balance approach gives the most accurate estimation of the total cumulative mass passing through the CP (9975 kg), a percent difference may be calculated for any run of the RBCA. For example, implementation of the RBCA using base-case control parameters and pressure heads from the System 1 homogeneous simulation results in a total cumulative mass of 9521 kg with a percent difference of 4.66 %. The relatively low percent difference is considered acceptable for the validation of the RBCA.

Additional runs of the RBCA were made to better understand the sensitivity of the RBCA to changes in the control parameters. The purpose of the first of these runs was to determine the total cumulative mass passing through the CP when the System 2 mesh is reconstructed to match the horizontal nodal placement of System 1. Therefore, all error introduced during the reconciliation of the two meshes is eliminated. The total cumulative mass for the error free case is 9,535 kg with a percent difference of 4.51 %. This is a 0.15 % drop from the percent difference calculated using the base-case control parameters. The next run of the RBCA examined the impact of changing the control parameters to allow for a higher resolution of the fluid flux distribution to be captured by the RBCA. The change in control parameters includes a maximum resolution level of 5, a maximum percent difference of 0.01 % and a lower mass limit of 1 kg. The resulting total cumulative mass is 9,536 kg with a percent difference of 4.50 %. This modest improvement (0.01 % difference) between the error free and higher resolution RBCA runs implies that the base values of the control parameters are effective in regulating the level of mesh reconciliation error.

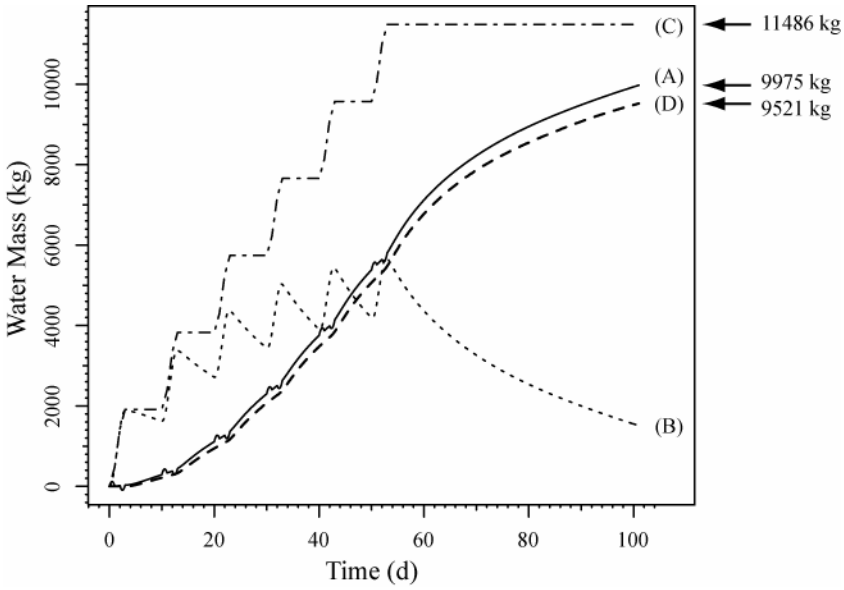

Figure 5.3: An estimate of the cumulative mass passing through the CP (A) is determined by subtracting the estimated change in water mass above the CP (B) from the cumulative mass of water infiltrating into the system from the ground surface (C). A validation of the RBCA is made by comparing (A) with the cumulative mass passing through the CP determined by the RBCA (D).

A major design issue when implementing the coupled systems approach is the placement of the lower horizontal System 1 boundary. Specifically, how far below the CP should the lower boundary be placed so as to minimize the influence of the lower boundary condition on the timing and distribution of flow and transport through the CP? Figure 5.4 shows the water mass flux through the CP over time for three different locations of the System 1 lower boundary. The three locations are defined in terms of the depth below the CP and specified as 0.5 m, 1.5 m and 2.5 m.

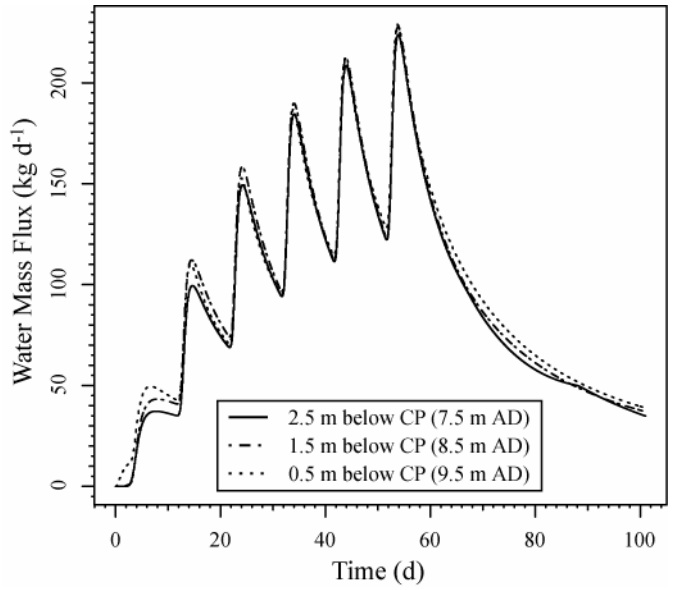

Figure 5.4: The sensitivity of the RBCA to changes in the location of the homogeneous System 1 lower boundary. The water mass flux is shown for lower boundary placements of 2.5 m, 1.5 m and 0.5 m below the CP.

The greatest deviation in water mass flux over time for the three lower boundary locations is during the early stages of the simulation. These early deviations are attributed to the sensitivity of the numerical model to changes in the initial pressure head distribution. For simulation times greater than 60 days the impact of the lower boundary location is also apparent. A reduction in the distance between the System 1 lower boundary and the CP results in a decreased drainage rate. The decrease in the drainage rate is attributed to the use of a free drainage boundary condition at the System 1 lower boundary. One of the side effects of a free drainage boundary condition is the buildup of groundwater behind the boundary, a phenomenon that is exasperated by high percolation rates near the boundary. Therefore, a reduction in the distance between the lower boundary and the CP results in an increase in the buildup of groundwater behind the lower boundary and a decrease in the drainage rates through the CP. The total

cumulative mass passing through the CP for a range of different System 1 lower boundary locations is summarized in Table 3.

Table 3: Total mass through the CP varying the location of the homogeneous System 1 lower boundary.

Depth Below CP	Distance Above Datum	Total Mass Through CP
2.5 m	7.5 m	9521 kg
2.0 m	8.0 m	9839 kg
1.5 m	8.5 m	9862 kg
1.0 m	9.0 m	9926 kg
0.5 m	9.5 m	10001 kg

5.2 System 1 Heterogeneous Flow and Transport Simulation

Results are presented for the System 1 heterogeneous flow and transport simulation. The heterogeneous media realization for System 1 is described in Figure 3.8. Figure 5.5 gives the conservative tracer concentration distribution within vertical cross-sections (y = 5 m and x = 5 m) after 25, 45 and 65 days of simulation. The solute profiles at these times exhibit a highly variable, jagged character typical of flow and transport in heterogeneous media (Phillips, 1994). Solute transport through the partially saturated media is advection dominated. Preferential flowpaths, in which small areas of the subsurface carry large portions of the flow, lead to the high spatial variability in the concentration distribution.

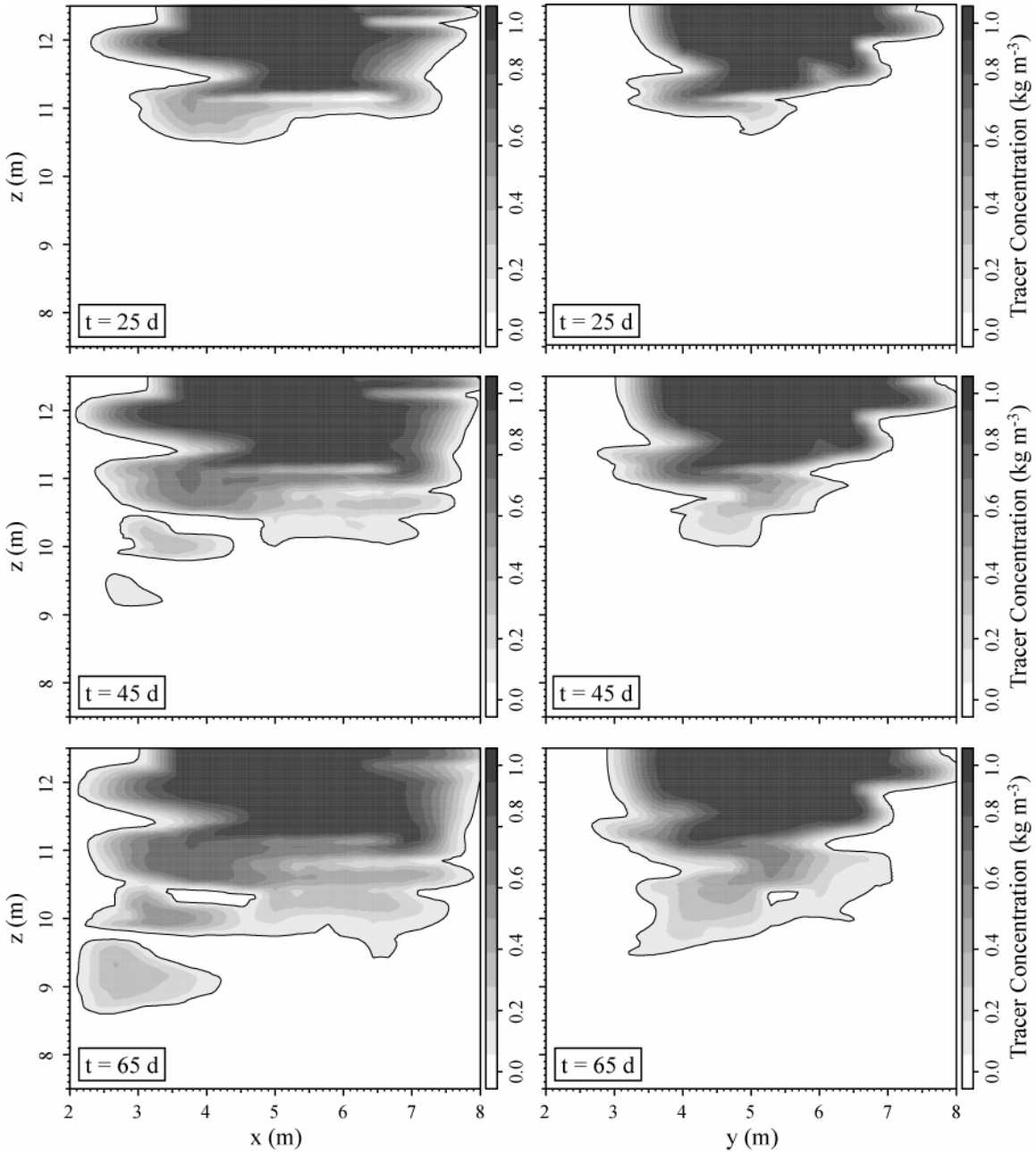

Figure 5.5: The tracer concentration distributions within vertical cross-sections (y = 5 m and x = 5 m) of a heterogeneous realization of System 1 after 25, 45 and 65 days of simulation.

Figure 5.6 gives the tracer concentration distribution within the CP (z = 10 m) after 25, 45 and 65 days of simulation. Accompanying each of the concentration distributions is the transport recharge boundary condition for identical simulation times.

The transport recharge boundary condition, a transient concentration specified for each element face in the System 2 recharge boundary, is determined from the RBCA using pressure heads and concentrations from a System 1 heterogeneous simulation. A comparison of the concentration distributions demonstrates the capability of the RBCA to accurately represent the concentrations of a System 1 simulation within the transport recharge boundary condition of a System 2 simulation. Additionally, the distribution comparison shows the tracer concentration within the CP increasing over time.

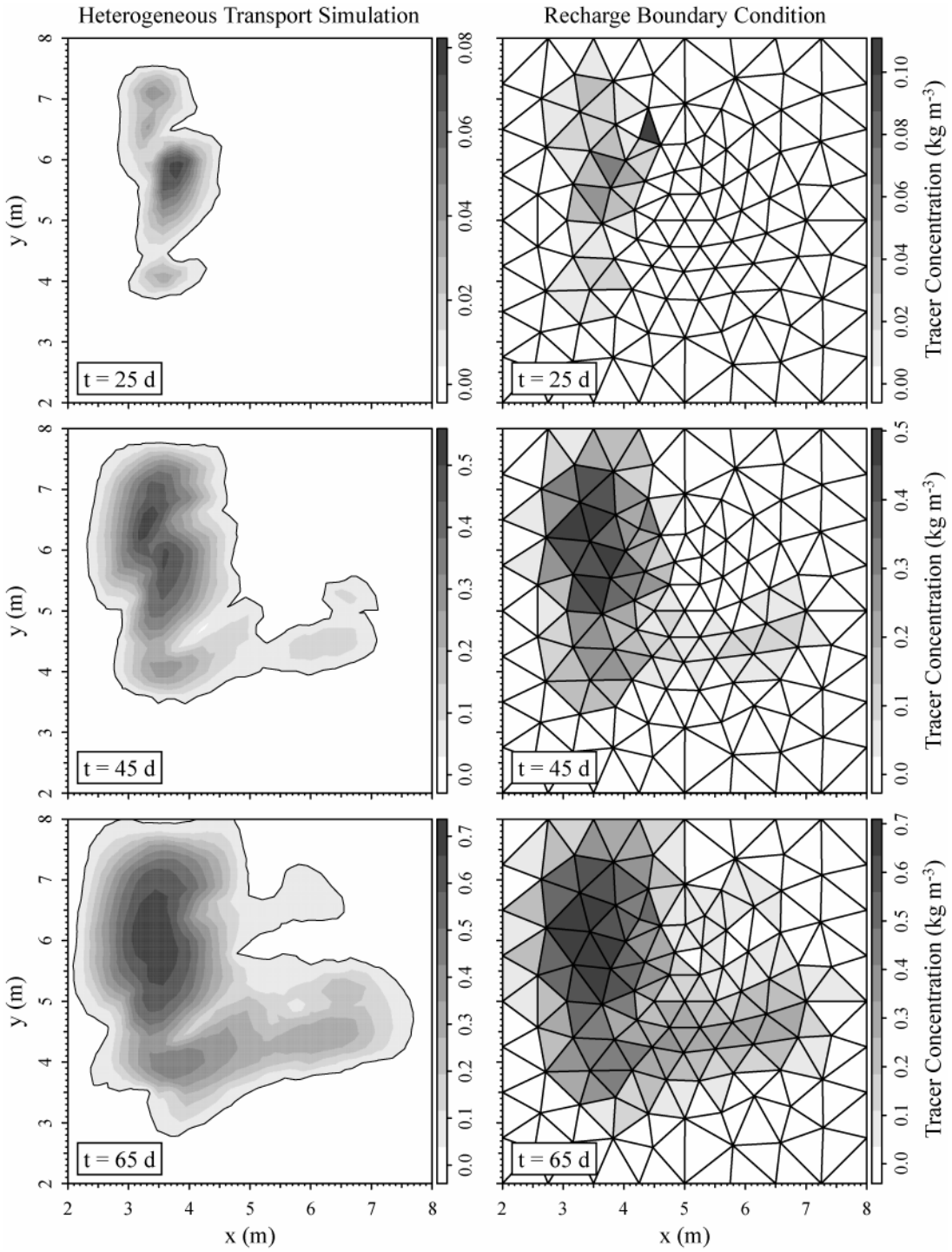

Figure 5.6: The tracer concentration distributions and recharge boundary condition within a horizontal cross-section (z = 10 m) of a heterogeneous realization of System 1 after 25, 45 and 65 days of simulation.

Implementation of the RBCA using base-case control parameters and the simulation results of a System 1 heterogeneous flow and transport simulation produces the recharge boundary condition for System 2, where a transient fluid flux and tracer concentration is generated for each element face in the System 2 recharge boundary. Figure 5.7 shows the water mass flux through the CP over time for both a homogeneous and heterogeneous simulation. The mass flux over time is characterized by incremental flux peaks, corresponding to each of the six infiltration cycles, followed by a long period of drainage.

The attenuated homogeneous flux peaks relative to the heterogeneous flux peaks are attributed to the distinct flow characteristics of homogeneous and heterogeneous media. Flow within the homogeneous media is evenly distributed with high moisture spreading in the transverse and lateral directions. The advancement of the wetting front into the initially dry soil allows for high water retention within the soil column. As moisture levels increase over time, the potential for water retention becomes less and the rate of downward percolation increases. This increase in the percolation rate is observed within the homogeneous flux peak responses, where the drainage rate and time to peak flux increase for each subsequent infiltration cycle. In contrast, the irregular flow within the heterogeneous media produces little moisture spreading, where high water transmissions through the preferential pathways result in rapid flux peak responses whose shape and magnitude remain somewhat constant over time.

After 100 days of simulation, water continues to pass through the CP, albeit at a very slow rate. Ideally, all drainage within the system would cease before ending the

System 1 simulation, thus insuring the most accurate representation of recharge within the System 2 simulation. For this dissertational research, however, the computational costs associated with a longer System 1 simulation were deemed unacceptable. During the later stages of drainage ($t > 80$ d), there is a convergence between the mass flux rates for the homogeneous and heterogeneous simulations. This convergence in mass flux illustrates the insignificance of the preferential pathways under low flow conditions.

The total mass of water passing through the CP during the heterogeneous simulation is 14,253 kg. Concern over the total mass value is raised due to a 2,678 kg exceedance of the total infiltrated mass. The mass exceedance error is believed to have originated from the numerical approximation of the Darcian flow through the unsaturated soil (Equation 4.2). Warrick (1991) found that the error in the numerical approximation can be alarmingly high for large pressure head gradients and is directly linked to the form of the numerical approximation (e.g. arithmetic, geometric, upstream averages). The form implemented within the RBCA merits of further consideration.

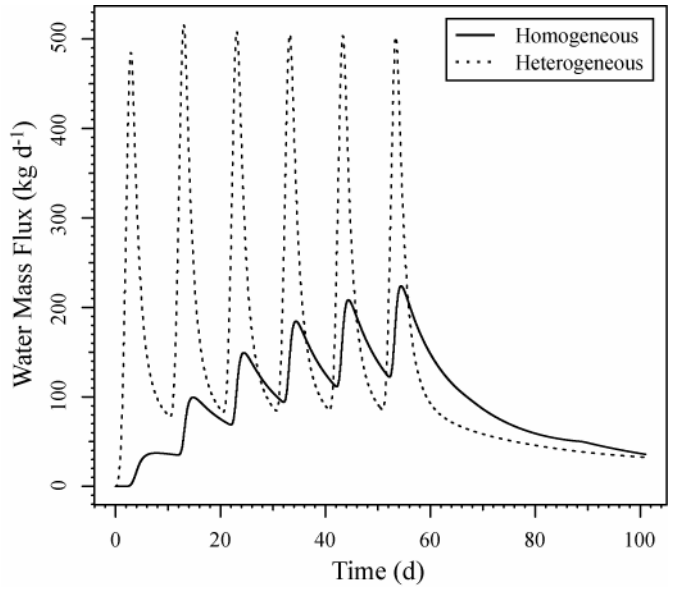

Figure 5.7: The water mass flux through the CP over time for homogeneous and heterogeneous soil conditions.

A series of RBCA runs were conducted for each of the control parameters (i.e. the maximum resolution level, maximum percent difference, lower mass limit and gradient spatial step) to better understand the sensitivity of the algorithm to incremental changes in the parameters (Figure 5.8). For example, the total fluid mass passing through the CP is calculated for four different maximum resolution levels while holding all other control parameters constant (i.e. base-case conditions). The functional relationship between total fluid mass and maximum resolution level provides a mechanism for evaluating the sensitivity of the RBCA. The analysis, however, assumes a one-to-one relationship between the varied control parameter and the RBCA solution, thus, neglecting all interdependencies between the control parameters. While this assumption is not strictly valid, the analysis is believed to provide an adequate means for evaluating the algorithms sensitivity.

Results for the sensitivity analysis are shown in Figure 5.8. The RBCA sensitivity is greatest for changes in the gradient spatial step size, Δz. Recall, that the numerical approximation of Darcian flow (Equation 4.2) is dependent on Δz. The accuracy of the approximation is reliant upon a sufficiently small value of Δz. The excessive amounts of total fluid mass corresponding to $\Delta z > 0.05$ m clearly shows the error associated with Δz being too large and illustrates the sensitivity of the algorithm to Darcian flow approximations. A suggested Δz value is the mesh's vertical spatial step size within the vicinity of the CP.

The sensitivity analysis is system-specific and highly dependent on base-case conditions. Therefore, a sensitivity analysis is recommended for any new implementation of the coupled systems modeling approach. That said, the general findings for the sensitivity analysis are as follows: (A) A higher maximum resolution level provides a moderate improvement in accuracy and a significant increase in computational time. (B) A small lower mass limit provides a high degree of accuracy at a relatively low computational cost. (C) An increase in the maximum percent difference allows for substantial computational savings with little degradation to the algorithm's solution. (D) There is a strong interdependency between the lower mass limit and the maximum percent difference. A recommended procedure is setting the lower mass limit to a small percentage of the total mass of water infiltrating through the ground surface and using the maximum percent difference to control the level of accuracy within the recharge boundary condition.

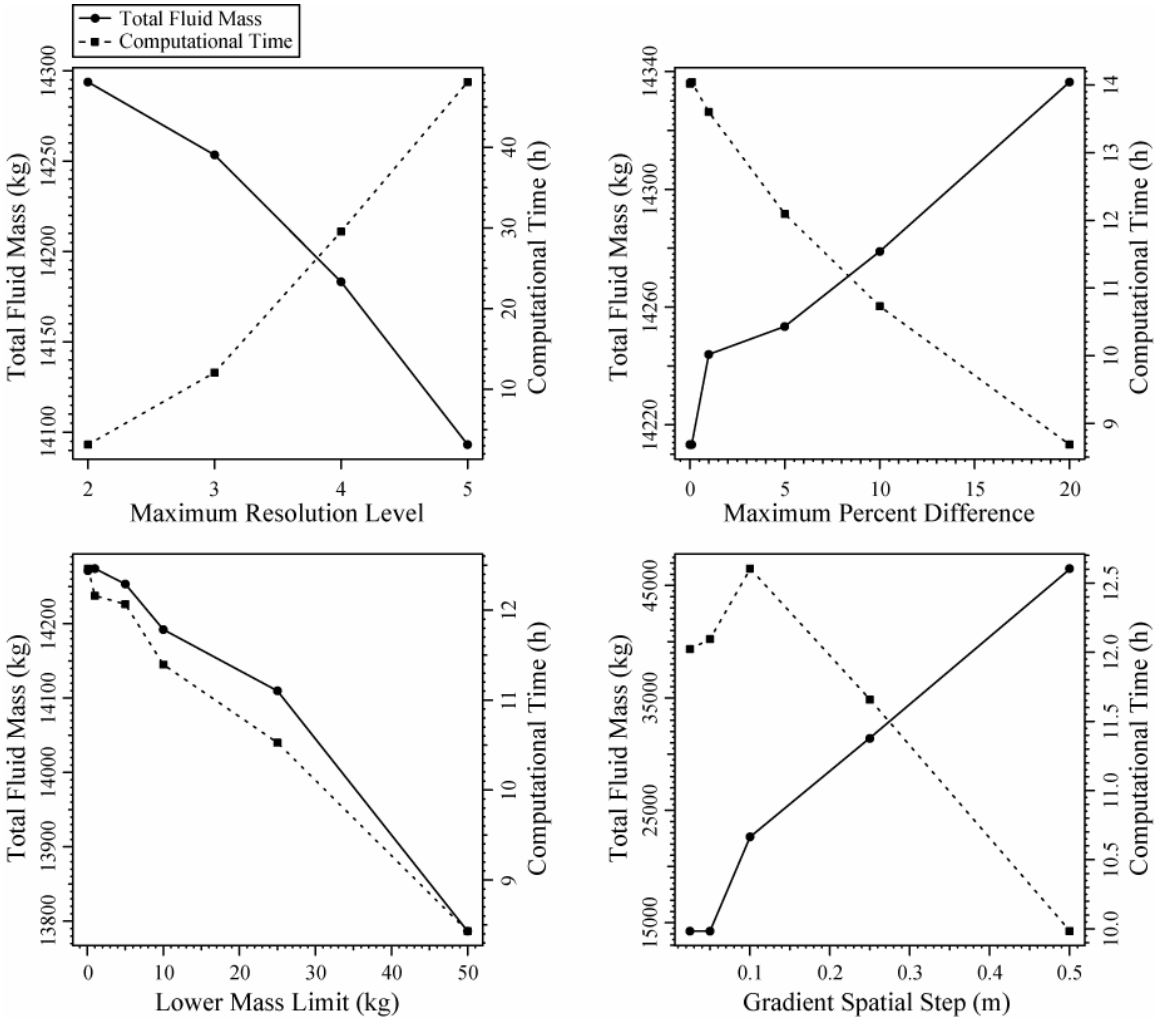

Figure 5.8: Sensitivity of the RBCA to variations in the maximum resolution level, maximum percent difference, lower mass limit and gradient spatial step (note the differences in scale).

The adaptive spatial mesh (Section 4.1) generated during the execution of the RBCA is dependent on the control parameters (i.e. a change in the control parameters produces a change in the adaptive spatial mesh). Figure 5.8 shows the sensitivity of the adaptive spatial mesh to changes in the maximum resolution level and maximum percent difference. All non-varied control parameters are set constant at base-case conditions. As expected, an increase in the maximum level of resolution produces a higher mesh

density, whereas, a reduction in the maximum percent difference allows for greater mesh refinement over a larger area.

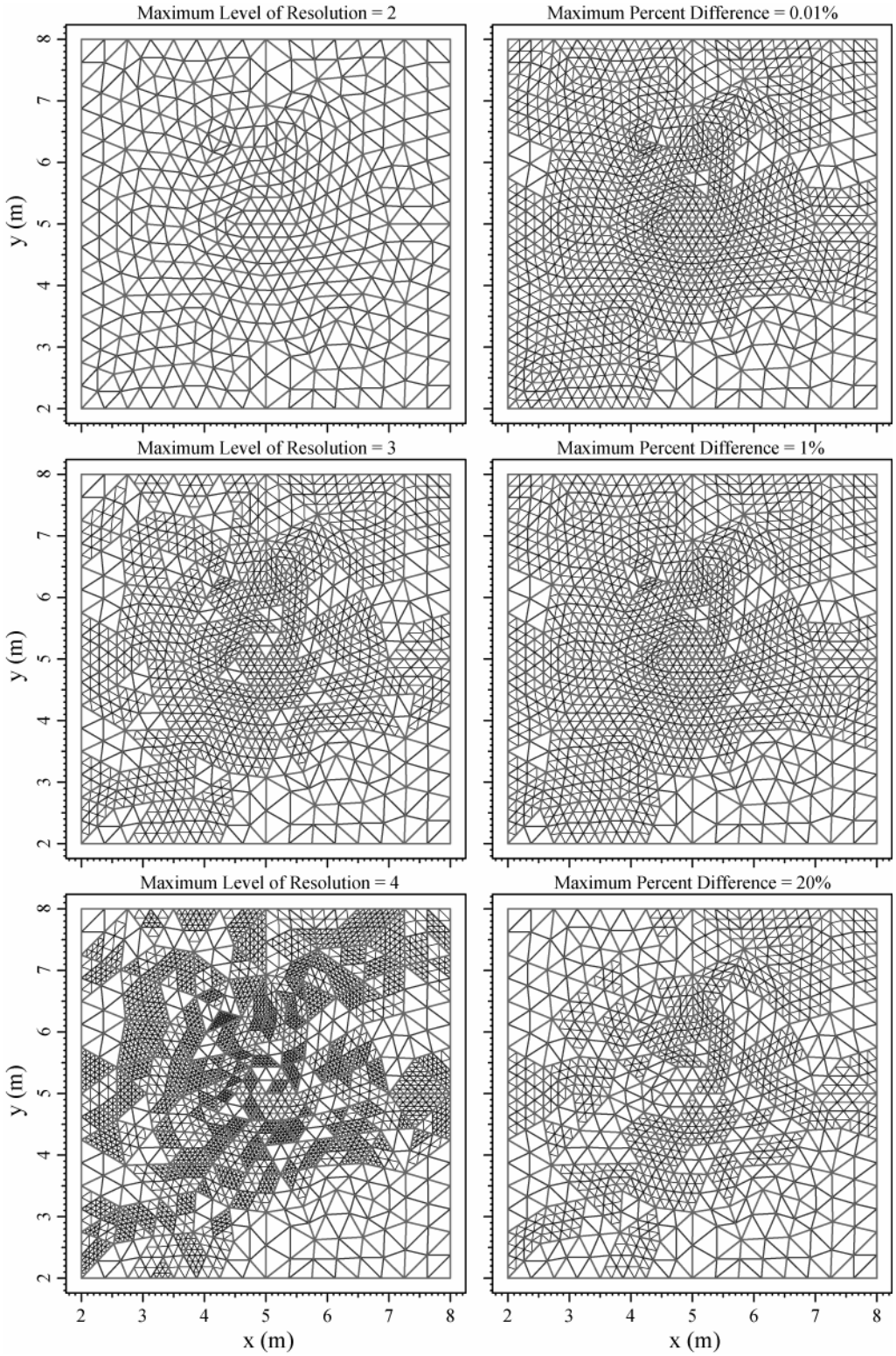

Figure 5.9: Sensitivity of the Adaptive Spatial Mesh Algorithm to variations in the maximum resolution level and maximum percent difference.

5.3 System 2 Flow and Transport Simulation

Results are presented for the System 2 flow and transport simulation. The System 2 recharge boundary condition is constructed with the RBCA using base-case control parameters and the simulation results from a System 1 heterogeneous flow and transport simulation. Figure 5.10 and 5.11 show the tracer concentration distributions within a vertical (y = 5 m) and horizontal (z = 9 m) cross-section of the System 2 domain after 100, 2500 and 5000 days of simulation, respectively. The vertical cross-section results are less demonstrative because the infiltration time used here (100 d) was insufficient to drive the recharging water deep into the aquifer. However, the horizontal view captures the plume dynamics for this system well. The horizontal cross-section is located just beneath the water table. After 100 days of simulation (corresponding with the end of the System 1 simulation) the recharge boundary condition is inactivated with no new solute entering into the system. The solute plume is then transported by advection and dispersion with advective transport governed by the level of mounding below the recharge boundary and the aquifer's natural gradient. Plume migration is characterized by observing the spatial concentration distributions after 100, 2500 and 5000 days.

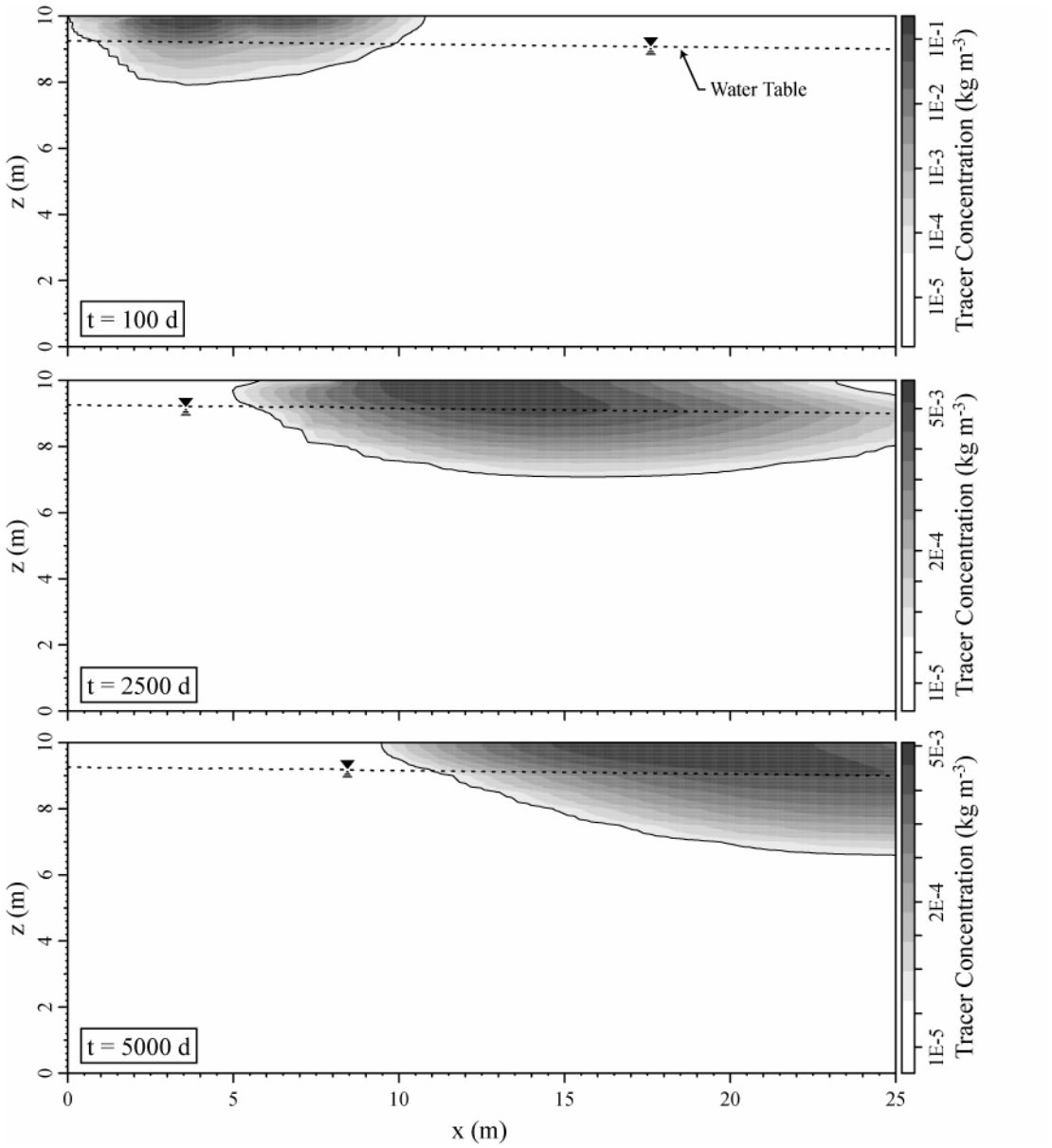

Figure 5.10: The tracer concentration distributions within a vertical cross-section (y = 5 m) of System 2 after 100, 2500 and 5000 days of simulation (note log scale for concentration).

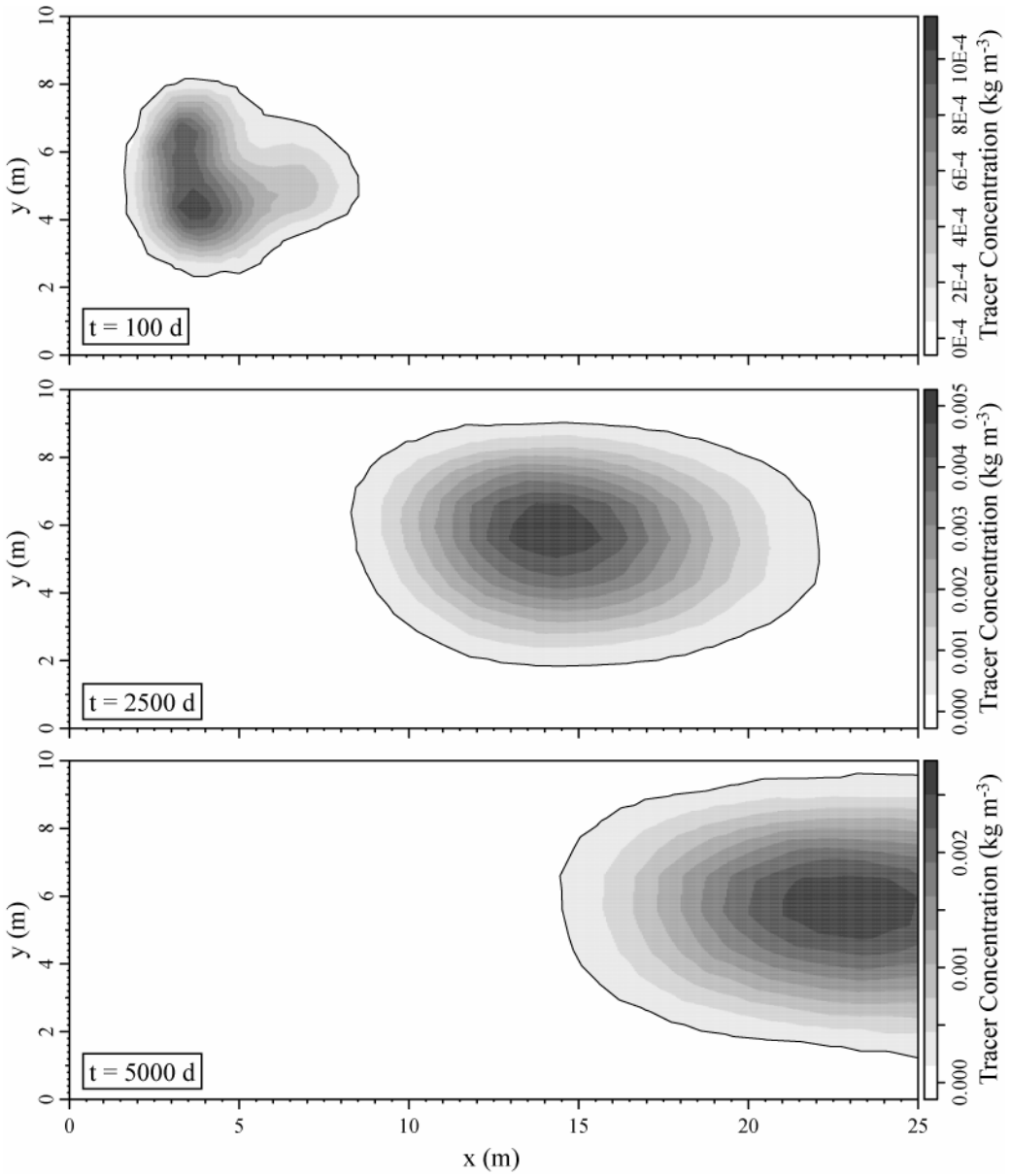

Figure 5.11: The tracer concentration distributions within a horizontal cross-section (z = 9 m) of System 2 after 100, 2500 and 5000 days of simulation.

6 CONCLUSIONS

A numerical approach is presented in which unsaturated and saturated zone flow and transport processes are decoupled. A method referred to as the Recharge Boundary Construction Algorithm (RBCA) is employed to transfer fluid and solute mass from the unsaturated domain into the saturated domain. Numerical simulations of flow and transport were employed in order to validate the RBCA. The dual systems approach will be useful in studying a host of problems in the fields of environmental engineering, water resources management, and hydrogeologic science. Specific systems that could benefit from the approach include those associated with artificial recharge, aquifer storage and recovery, and disposal of wastes by land or pond application. The main findings for the dissertational research may be summarized as follows:

1. The coupled systems approach addresses the high computational costs associated with a combined vadose zone-groundwater flow and transport model.
2. The RBCA was validated for a System 1 homogeneous flow simulation using a mass balance approach.
3. Problems with mass balance arise for heterogeneous soil conditions in the vadose zone. The errors in RBCA mass conservation are attributed to the Darcian flow approximation for fluid movement through the control plane.
4. Implementation of the RBCA requires a sensitivity analysis on the user-defined control parameters.
5. There is a strong interdependency between the lower mass limit and the maximum percent difference. A recommended procedure is setting the lower mass limit to a

small percentage of the total mass of water infiltrating through the ground surface and using the maximum percent difference to control the level of accuracy within the recharge boundary condition.

6. Simulated distribution patterns for pressure head and concentration were preserved within the recharge boundary condition.

7 REFERENCES

Aris, R., *Vectors, Tensors and the Basic Equations of Fluid Mechanics*, Prentice-Hall, New Jersey, 1962.

Bear, J., *Dynamics of Fluids in Porous Media, Dover Publications*, Inc., New York, 1988.

Carroll, D. L., *FORTRAN Genetic Algorithm (GA)*, http://cuaerospace.com/carroll/ga.html, Version 1.7a, 2001.

Cussler, E. L., *Diffusion: Mass Transfer in Fluid Systems*, Cambridge University Press, New York, 1984.

Darcy, H., *Les Fontaines Publiques de la Ville de Dijon*, Dalmont, Paris, 1856.

Destouni, G., and W. Graham, Solute transport through an integrated heterogeneous soil-groundwater system, *Water Resources Research*, 31(8), 1935-1944, 1995.

Foussereau, X., W. D. Graham, G. A. Akpoji, G. Destouni, and P. S. C. Rao, Solute transport through a heterogeneous coupled vadose-saturated zone system with temporally random rainfall, *Water Resources Research*, 37(6), 1577-1588, 2001.

Hantush, M. S., Growth and decay of ground water mounds in response to uniform percolation, *Water Resources Research*, 3(1), 227-235, 1967.

Healy, R. W., Simulation of solute transport in variably saturated media with supplemental information on modifications to the U.S. Geological Survey's computer program VS2D, *U.S. Geological Survey Water-Resources Investigations Report 90-4025*, 125 p., 1990.

Ihaka, R. and R. Gentleman, R: A language for data analysis and graphics, *Journal of Computational and Graphical Statistics*, 5(3), 299-314, 1996.

Isaaks, E. H. and R. M. Srivastava, *An introduction to Applied Geostatistics*, Oxford University Press, 1989.

Lapidus, L. and G. F. Pinder, *Numerical Solution of Partial Differential Equations in Equations in Science and Engineering*, John Wiley & Sons, Inc., 1982.

Lappala, E. G., W. R. Healy, and E. P. Weeks, Documentation of computer program VS2D to solve the equations of fluid flow in variably saturated porous media,

U.S. Geological Survey Water- Resources Investigations Report 83-4099, 184 p., 1987.

Latinopoulos, P., Analytical solutions for strip basin recharge to aquifers with caucy boundary conditions, *Journal of Hydrology*, 83, 197-206, 1986.

Li, B., and T.-C. J. Yeh, Sensitivity and moment analyses of head in variably saturated regimes, *Advances in Water Resources*, 21(6), 477-485, 1998.

Lin, H-C., D. Richards, C. Talbot, G. T. Yeh, J-R. Cheng, H-P. Cheng, and N. Jones, *FEMWATER: A Three-Dimensional Finite Element Computer Model for Simulating Density-Dependent Flow and Transport in Variably Saturated Media*, US Army Engineer Waterways Experimental Station Technical Report CHL-97-12, 1997.

Lu, Z., and D. Zhang, Solute spreading in nonstationary flows in bounded, heterogeneous unsaturated-saturated media, *Water Resources Research*, 39(3), 1049, doi:10.1029/2001WR000908, 2003.

Manglik, A., and S. N. Rai, Two-dimensional modeling of water table fluctuations due to time-varying recharge from rectangular basin, *Water Resources Management*, 12, 467-475, 1998.

Manglik, A., and S. N. Rai, Modeling of water table fluctuations in response to time-varying recharge and withdrawal, *Water Resources Management*, 14, 339-347, 2000.

Marino, M. A., Artificial ground water recharge – II, rectangular recharging area, *Journal of Hydrology*, 26, 29-37, 1975.

McCord, J. T., Application of second-type boundaries in unsaturated flow modeling, *Water Resources Research*, 27(12), 3257-3260, 1991.

McCord, J. T., C. A. Gotway and S. H. Conrad, Impact of geologic heterogeneity on recharge estimation using environmental tracers: Numerical modeling investigation, *Water Resources Research*, 33(6), 1229-1240, 1997.

Morel-Seytoux, H. J., C. Miracapillo, and M. J. Abdulrazzak, A reductionist physical approach to unsaturated aquifer recharge from a circular spreading basin, *Water Resources Research*, 26(4), 771-777, 1990.

Mualem, Y., A new model for predicting the hydraulic conductivity of unsaturated porous media, *Water Resources Research*, 12(3), 513-522, 1976.

Pebesma, E. J. and C. G. Wesseling, Gstat, a program for geostatistical modeling, prediction and simulation, *Computers and Geosciences*, 24(1), 17-31, 1998.

Phillips, F. M., Environmental tracers for water movement in desert soils of the American southwest, *Soil Science Society of America Journal*, 58, 15-24, 1994.

Pinder, G. F. and W. G. Gray, *Finite Element Simulation in Surface and Subsurface Hydrology*, Academic Press, New York, 1977.

Rao, N. H., and P. B. S. Sarma, Recharge to finite aquifer from strip basins, *Journal of Hydrology*, 66, 245-252, 1983.

Richards, L. A., Capillary conduction of liquids through porous mediums, *Physics*, 1, 318-333, 1931.

Rubin, Y. and A. Bellin, The effects of recharge on flow nonuniformity and macrodispersion, *Water Resources Research*, 30(4), 939-948, 1994.

Ruan, F. and D. McLaughlin, An investigation of Eulerian-Lagrangian methods for solving heterogeneous advection-dominated transport problems, *Water Resources Research*, 35(8), 2359-2373, 1999.

Russo, D., J. Zaidel, and A Laufer, Numerical analysis of flow and transport in a combined heterogeneous vadose zone-groundwater system, *Advances in Water Resources*, 24, 49-62, 2001.

Sanford, W., Recharge and groundwater models: an overview, *Hydrogeology Journal*, 10, 110-120, 2002.

Serrano, S. E., The form of the dispersion equation under recharge and variable velocity, and its analytical solution, *Water Resources Research*, 28(7), 1801-1808, 1992.

Sudicky, E. A., J. A. Cherry, and E. O. Frind, Migration of contaminants in groundwater at a landfill: A case study, 4, A natural-gradient dispersion test, *Journal of Hydrology*, 63, 81-108, 1983.

Sumner, D. M., and L. A. Bradner, Hydraulic characteristics and nutrient transport and transformation beneath a rapid infiltration basin, *USGS Water-Resources Investigations Report No. 95-4281*, Reedy Creek Improvement District, Orange County, Fla., U. S. Geological Survey, Tallahassee, Fla., 1996.

Sumner, D. M., D. E. Rolston, and M. A. Mariño, Effects of unsaturated zone on ground-water mounding, *Journal of Hydrologic Engineering*, 4(1), 65-69, 1999.

Sun, A. Y., and D. Zhang, Prediction of solute spreading during vertical infiltration in unsaturated, bounded heterogeneous porous media, *Water Resources Research*, 36(3), 715-723, 2000.

Sun, N.-Z., *Mathematical Modeling of Groundwater Pollution*, Springer, New York, 1996.

Swamee, P. K., and C. S. P. Ojha, Ground-water mound equation for rectangular recharge area, *Journal of Irrigation and Drainage Engineering*, 123(3), 215-217, 1997.

van Genuchten, M. Th., A closed-form equation for predicting the hydraulic conductivity of unsaturated soils, *Soil Science Society of America Journal*, 44, 892-898, 1980.

Warrick, A. W., Numerical approximations of Darcian flow through unsaturated soil, *Water Resources Research*, 27(6), 1215-1222, 1991.

Zhang, D., and Z. Lu, Stochastic analysis of flow in a heterogeneous unsaturated-saturated system, *Water Resources Research*, 38(2), 1018, doi:10.1029/2001WR000515, 2002.

Zlotnik, V., and G. Ledder, Groundwater flow in a compressible unconfined aquifer with uniform circular recharge, *Water Resources Research*, 28(6), 1619-1630, 1992.

Zlotnik, V., and G. Ledder, Groundwater velocity in an unconfined aquifer with rectangular areal recharge, *Water Resources Research*, 29(8), 2827-2834, 1993.

Zomorodi, K., Evaluation of the response of a water table to a variable recharge rate, *Hydrological Sciences Journal*, 36, 67-78, 1991.